



FACULTY
OF MECHANICAL
ENGINEERING
CTU IN PRAGUE

Department of material engineering

Vliv deformace na strukturu a vlastnosti slitiny Al-Mg-Si

Influence of deformation on structure and properties of Al-Mg-Si alloy

MASTER THESIS

2020

Bc. Radek Bednář

Study program: N 2301 STROJNÍ INŽENÝRSTVÍ
Field of study: 3911T037 Material and Production Engineering
Supervisor: Ing. Jakub Horník, Ph.D.
Dr. Ir. Husaini Ardy

I. OSOBNÍ A STUDIJNÍ ÚDAJE

Příjmení: **Bednář** Jméno: **Radek** Osobní číslo: **438600**
Fakulta/ústav: **Fakulta strojní**
Zadávající katedra/ústav: **Ústav materiálového inženýrství**
Studijní program: **Strojní inženýrství**
Studijní obor: **Výrobní a materiálové inženýrství**

II. ÚDAJE K DIPLOMOVÉ PRÁCI

Název diplomové práce:

Vliv deformace na strukturu a vlastnosti slitiny AlMgSi

Název diplomové práce anglicky:

Influence of deformation on structure and properties of AlMgSi alloy

Pokyny pro vypracování:

Literární rešerše - vliv teploty a deformace na odpevňovací procesy Al slitin
Problematika slitin AlMgSi
Experimentální část:
Vyhodnocení mikrostrukturálních charakteristik vybraných stavů materiálů po deformaci s použitím světelné mikroskopie a
řádkovací elektronové mikroskopie (metoda EBSD)
Diskuse výsledků a závěry

Seznam doporučené literatury:

- [1] MICHNA, Štefan. Encyklopedie hliníku. Prešov: Adin, 2005. ISBN 80-89041-88-4.
- [2] SEDLÁČEK, Vladimír. Zotavení a rekrystalizace. Praha: Academia, 1985.
- [3] Joseph R. Davis, J.R. Davis & Associates, Aluminum and aluminum alloys. ASM International. Handbook Committee ASM International, 1993, ISBN 13: 9780871704962

Jméno a pracoviště vedoucí(ho) diplomové práce:


Ing. Jakub Horník, Ph.D., ústav materiálového inženýrství FS


Jméno a pracoviště druhé(ho) vedoucí(ho) nebo konzultanta(ky) diplomové práce:


Datum zadání diplomové práce: **22.10.2019**

Termín odevzdání diplomové práce: **08.01.2020**

Platnost zadání diplomové práce: _____


Ing. Jakub Horník, Ph.D.
podpis vedoucí(ho) práce


prof. RNDr. Petr Špatenka, CSc.
podpis vedoucí(ho) ústavu/katedry

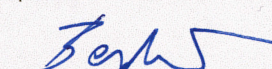

prof. Ing. Michael Valášek, DrSc.
podpis děkana(ky)

III. PŘEVZETÍ ZADÁNÍ

Diplomant bere na vědomí, že je povinen vypracovat diplomovou práci samostatně, bez cizí pomoci, s výjimkou poskytnutých konzultací.
Seznam použité literatury, jiných pramenů a jmen konzultantů je třeba uvést v diplomové práci.

30.10.2019

Datum převzetí zadání



Podpis studenta

DECLARATION

I declare that I have done this work independently and solely using the sources and literature listed in the list of cited sources.

In Prague on: 8.1.2020

Signature: 

ABSTRACT

This thesis deals with the influence of deformation parameters on the structure and mechanical properties of the alloy EN AW 6082. Two different semi-finished products were compared - extruded semi-finished products and HCM semi-finished products. The structure and mechanical properties of these semi-finished products in various variants of deformation and with or without heat treatment were evaluated. This thesis was created in cooperation with Strojmetal Aluminum Forging s.r.o.

KEY WORDS

ALUMINUM ALLOYS, Al-Mg-Si, EN AW 6082, HCM, EXTRUSION, DEFORMATION PARAMETERS, RECRYSTALLIZATION, MECHANICAL PROPERTIES, MICROSTRUCTURE, EBSD

ANOTACE

Tato práce se zabývá vlivem deformačních parametrů na strukturu a mechanické vlastnosti slitiny EN AW 6082. Byly porovnány dva různé polotovary, polotovary vyrobené metodou průtlačného lisování a metodou HCM. Byla vyhodnocena struktura a mechanické vlastnosti těchto polotovarů v různých variantách deformace bez a s tepelným zpracováním. Tato práce byla vytvořena ve spolupráci se společností Strojmetal Aluminium Forging s.r.o.

KLÍČOVÁ SLOVA

HLINÍKOVÉ SLITINY, Al-Mg-Si, EN AW 6082, HCM, PRŮTLAČNÉ LISOVÁNÍ, PARAMETRY DEFORMACE, REKRYSTALIZACE, MECHANICKÉ VLASTNOSTI, MIKROSTRUKTURA, EBSD



ACKNOWLEDGEMENT

I would like to thank you to Ing. Jakub Horník, Ph.D. for valuable comments and expert advice on the content of this thesis. Furthermore, I would like to thank my co-workers, all employees of the Institute of Materials at CTU, who helped me to finish this thesis and all academic staff of ITB Bandung that helped me during my study.

TABLE OF CONTENTS

Introduction	10
Theoretical part.....	11
1 Property of aluminum and its alloys.....	11
1.1 Pure aluminum	11
1.2 Physical properties of aluminum	11
1.2.1 Divide of aluminum alloys.....	12
2 Series 6000	14
2.1 System Al-Mg-Si.....	14
2.2 Alloying elements of alloys series 6000.....	15
2.3 Alloy EN AW 6082	16
3 Strengthening mechanisms	18
3.1 Dislocation hardening	18
3.2 Grain boundary hardening	19
3.3 Hardening by alloying	20
3.4 Precipitation hardening.....	21
4 Recovery and recrystallization	24
4.1 Recovery	26
4.1.1 Recovery of point defects	26
4.1.2 Polygonization	26
5 Recrystallization	28
5.1 Mechanism and kinetics of recrystallization.....	28
5.1.1 Primary recrystallization.....	28
5.1.2 Secondary recrystallization	31
5.2 Factors affecting recrystallization	31
5.2.1 Material and its purity.....	31
5.2.2 Influence of precipitation and grain size	32
5.2.3 Extent of deformation	33
5.2.4 Temperature of deformation	33
5.2.5 Dynamic recrystallization and recovery	33
6 Plastic deformation	35
6.1 Plastic deformation and its mechanisms.....	35
6.2 Slip mechanism.....	35
6.3 Twinning mechanism	36
6.4 Deformation energy.....	36
6.5 Deformation structure	37
6.6 Homogeneity of deformation	37
6.7 Influence of temperature on plastic deformation.....	38
6.8 Deformation resistance.....	38

7	Heat treatment of aluminum alloys	39
7.1	Annealing	39
7.2	Solution heat treatment.....	40
7.2.1	Solution annealing.....	40
7.2.2	Aging.....	40
7.2.2.1.	Artificial aging.....	40
	Experimental part.....	42
8	Samples preparation.....	43
8.1	Input parameters of semi-finished products	43
8.1.1	HCM.....	43
8.1.2	Extrusion.....	43
8.2	Free forging of the samples	44
8.3	The variants of the free forging	44
8.4	The parameters of free forging.....	45
8.5	The parameters of heat treatment	45
9	The evaluation of the macrostructure	46
10	Metallography	47
10.1	The cutting of the material.....	47
10.2	The pressing	48
10.3	The grinding and polishing	48
10.4	The etching.....	49
11	The tensile test.....	50
12	The evaluation of the microstructure.....	54
12.1	The light microscopy	54
12.2	Electron backscatter diffraction.....	62
13	The hardness of the samples	68
13.1	Extruded semi-finished products	69
13.2	HCM semi-finished products	72
13.3	Comparison of the hardness test results	75
	Conclusion.....	77
	Bibliography.....	79
	List of figures.....	81
	List of tables.....	82

LIST OF USED ABBREVIATIONS AND SYMBOLS

Abbreviation Symbol	Expression	Unit
kgf	kilogram-force	N
K12	Face-centered cubic lattice	-
NA	Natural aging	-
AA	Artificial aging	-
R_{p0.2}	Yield strength	MPa
R_m	Ultimate tensile strength	MPa
A₅	Ductility of short test rod	%
A₁₀	Ductility of long test rod	%
T_M	Melting point	K
HCM	Horizontal casting material	-
EXT	Extrusion	-
ε_h	Deformation degree	%
ε_{h0}	Degree of discrete deformation	%
A	Ductility	%
Z	Area reduction	%
PO	Transection	-
PR	Cross section	-
EBSD	Electron backscatter diffraction	-
BSE	Back-scattered electrons	-
UFG	Ultrafine Grained	-



SPD	Severe plastic deformation	-
HKL	Miller indices	-
SEM	Scanning electron microscope	-
HAGB	High-angle grain boundary	-
LAGB	Low-angle grain boundary	-
HV	Vickers hardness	-
HV1	Vickers hardness – load 1 kgf	-
ØHV1	Average value of Vickers hardness – load 1 kgf	-
ΔHV1	Incremental value of Vickers hardness – load 1 kgf	-

Introduction

In the automotive industry, great emphasis is placed on reducing fuel consumption and resulting emissions. For this reason, we are looking for a ways to lighten the construction of the car. Therefore, aluminum alloys are increasingly used. In the automotive industry, these are mostly Al-Mg-Si alloys.

The thesis was initiated by Strojmetal Aluminum Forging s.r.o. Because of the topic is extensive, three people participated in the experimental part. Besides me, it was my colleagues Veronika Kozáková and Ing. Tom Procházka.

The subject of this master thesis is the observing of the influence of deformation and repeated deformation on recrystallization and mechanical properties of the alloy EN AW 6082, which is delivered in two different manufactured semi-finished products. Half of the semi-finished products were produced by extrusion and the other half by horizontal continuous casting (HCM). Semi-finished products were free forged to different degrees of deformation, discrete deformation was performed on a part of the samples. A sample with or without heat treatment was prepared for each degree of deformation.

The aim of the thesis is to evaluate the macrostructure. Microstructure evaluation on both light microscopy and EBSD. Evaluation of mechanical properties by tensile test and hardness measurement.

THEORETICAL PART

1 Property of aluminum and its alloys

1.1 Pure aluminum

Technically pure aluminum has an aluminum content 99% and above. The mechanical properties of aluminum are not sufficient for the vast majority of construction applications, and therefore its alloys are used which achieve significantly better properties. However, aluminum has excellent formability, conductivity and corrosion resistance. Therefore, pure aluminum is mainly used in the power industry for conductors and components of electrical installations. It is also used as a packaging foil because it is not toxic, and the formability allows the production of foils. Aluminum can also be used for cladding as a form of corrosion protection and is also used for lightly stressed parts for an attractive appearance. [1] [2]

1.2 Physical properties of aluminum

Tab. 1 lists some physical properties of aluminum. Aluminum has a cubic K12 grating, which makes aluminum and its alloys have good plastic properties both hot and cold environment. Slip planes are {111}, slip directions <110>.

Table 1 - Selected physical properties of aluminum [1]

Quantity	Value	Unit
Atomic number	13	-
Relative atomic mass	26,982	-
Crystal lattice	K12	-
Lattice parameter	0,404958	nm
Density	2.699 (20 °C)	$\text{g}\cdot\text{m}^{-3}$
Melting temperature	660.37 (Al 99,996%)	°C
Boiling point	2494	°C
Thermal conductivity	247 (25 °C)	$\text{W}\cdot\text{m}^{-1}\cdot\text{K}^{-1}$
Heat capacity	0.9	$\text{J}\cdot\text{g}^{-1}\cdot\text{K}^{-1}$
Volume change during crystallization	6.5	%
Electric resistance	26.2 (Al 99.99%; 20 °C)	$\mu\Omega\text{m}$
Superconductivity temperature	1.2	K
Modulus of elasticity	70	GPa

Tab. 2 shows the thermal expansion values of aluminum at different temperature intervals. These values are important for aluminum construction purposes.

Table 2 – The thermal expansion values at different temperature intervals [1]

Temperature interval [°C]	Average coefficient [$\mu\text{m}/\text{m}\cdot\text{K}$]
-200 to 20	18.0
-150 to 20	19.9
-50 to 20	21.8
20 to 100	23.6
20 to 200	24.5
20 to 300	25.5
20 to 400	26.4
20 to 500	27.4

1.2.1 Divide of aluminum alloys

Aluminum alloys can be divided according to the phase diagram with the alloying element. For simplicity, a binary diagram is shown in Fig. 1, but for alloys with multiple alloying elements, must be used multi-component diagrams, for example, a ternary diagram is used for two alloying elements. Aluminum alloys can be divided from two points of view, the eventualities of heat treatment and their utilization.

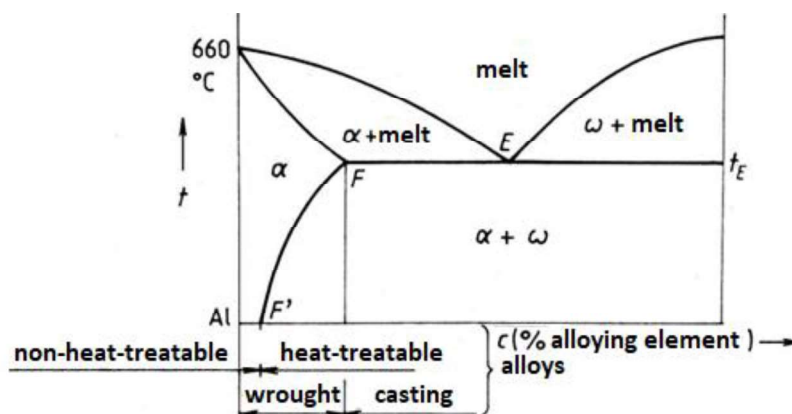


Figure 1 – Divide of aluminum alloys [3]

The first division in terms of heat treatment is the ability to solution heat treatment. According to Fig. 1, the alloy that can be solution heat treated must contain an enough alloying elements to dissolve the precipitates in solid solution α . The solution heat treated alloys are in the binary diagram Fig. 1 between points

F' and F. Non-solution heat treated alloys are located between pure aluminum and point F'.

The second division is their utilization. Alloys are divided into wrought and cast. For wrought alloys, it is desirable that plastic solid solution α predominates in their microstructure. In the binary diagram they are located between pure aluminum and point F. From point F onwards, these alloys are referred to cast. Cast alloys contain a greater number of alloying elements, which usually leads to the formation of hard and brittle phases that impair formability. To improve the cast ability, it is desirable to engender a eutectic. [2] [3]

The Tab. 3 shows how many alloying elements content the alloys which are used for forming and casting.

Table 3 - Maximum content of alloying elements [1]

Alloying element	Wrought alloys [%]	Casting alloys [%]
Cu	<6	<12
Mg	<8	<11
Mn	<2	<2
Si	<1	<25
Zn	<8	<6
Fe	<0,5	<1,6

2 Series 6000

The main alloying elements of the series are magnesium and silicon. These alloys have excellent formability and weldability, excellent corrosion resistance and good machinability. They are used as components in vehicles, bridge constructions and sports equipment. [1]

2.1 System Al-Mg-Si

The ternary system Al-Mg-Si is one of the simpler angling diagrams. The solid aluminum solution is in equilibrium with the Mg_2Si phase. Thanks to this phase, these alloys are heat-treatable, and in terms of mechanical properties, it depends on the amount of Mg_2Si phase. No other ternary phases were detected in this system, Al-Mg-Si. Stable phases of this system are shown in Tab. 4. Silicon occurs in ternary equilibria in elemental form. [1]

Table 4 – Solid phases in the Al-Mg-Si system [1]

	β	E	ζ		
Phase	Al_3Mg_2	$Al_{30}Mg_{23}$	$Al_{12}Mg_{17}$	Al_5Mg_4	Mg_2Si
T [°C]	< 450	450÷370	<460		<1085

The magnesium and silicon atoms in the aluminum solution attempt to form Mg_2Si phase precipitates. The maximum solubility of the Mg_2Si phase is 1.85% at 595 °C. In the Mg_2Si phase, magnesium and silicon are in a ratio of 1.73:1. If the Si content is higher than the Mg:Si concentration ratio = 1.73, the solubility of the Mg_2Si phase in the solid aluminum solution decreases. The ratio between magnesium and silicon is more important for the properties of alloys than the actual content of both elements. [1]

2.2 Alloying elements of alloys series 6000

In Tab. 5 are shown the intervals of alloying elements that occur in these aluminum alloys.

Table 5 - Alloying intervals for wrought alloys 6000 series [1]

Alloying element	Quantity [%]
Mg	0.2 – 1.5
Si	0.2 – 2.0
Mn	0 – 1.5
Cr	0 – 0.5
Cu	0 – 2.0
Zn	0 – 2.5
B	0 – 0.3
Ti	0 – 0.3
Zr	0 – 0.3
Pb	0 – 1.0
Bi	0 – 1.0
Sn	0 – 1.0

The following overview describes the effect of additional alloying elements for the 6000 series. [1] [4] [5]

Boron - softens the structure, increases the ability of Al to capture neutrons.

Bismuth - is added for better mechanical machinability.

Chromium - is added to make the recrystallization process more difficult and reduce the critical cooling rate, reducing electrical conductivity.

Copper - is added to increase strength properties, reducing corrosion resistance.

Manganese - is added to increase strength properties, increase recrystallization temperatures, grain refinement, blocking grain growth in case of its excretion in the form of dispersed precipitates and to suppress the excretion of Fe in the plate shape.

Lead - is added for better machinability, Al-Cu-Mg alloys may cause heat cracking due to segregation during recrystallization.

Tin - increases strength properties and speeds up the aging process.

Titanium - is added with boron to refine the structure. Fine intermetallic phases of TiB₂ are formed.

Zinc - increases strength properties.

Zirconium - creates fine precipitates that block recovery and recrystallization processes.

Depending on the amount of magnesium and silicon and their relative ratio, it can be divided into three groups.

In the first group, the total amount of silicon and magnesium does not exceed 1.5%. The two main elements are in an equilibrium Mg:Si ratio of 1.73 or with a slight excess of silicon. The first group includes alloy 6082, which is the subject of this thesis. The advantage of this alloy is that in solution annealing a temperature of just over 500 °C is sufficient and has a low sensitivity to the critical cooling rate during cooling. This means that it is possible to allow the alloy to cool in air after solution annealing. It achieves good strength and ductility and excellent corrosion resistance. [1] [4] [5]

The second group contains 1.5 % or more magnesium. Excess magnesium provides better corrosion resistance but deteriorates formability over alloys with excess silicon. In addition to silicon, other elements such as copper are added. Copper increases the heat treatment strength. Elements such as manganese, chromium and zirconium are used to obtain a fine grain structure. [1]

The third group contains more Mg₂Si phase than the first two groups. An excess of silicon increases the strength of the alloy, which contains 0.8 % Mg₂Si by 70 MPa, but worsens the weldability over the alloys of the first two groups. The addition of lead and bismuth improves machinability. [1] [5]

2.3 Alloy EN AW 6082

The main alloying elements are silicon, magnesium and manganese. The chemical composition of the alloy is shown in Tab. 6. [6]

Table 6 - Chemical composition of EN AW 6082 alloy in weight % [6]

Si	Fe	Cu	Mn	Mg	Cr	Zn	Ti	Al
0.7 – 1.3	0.5	0.1	0.4 - 1	0.6 – 1.2	0.25	0.2	0.1	residuals

This alloy is widely used in lightweight construction due to the combination of good strength and low weight. After a heat treatment, the yield strength value is at the level of steel S235. Other properties of this alloy are good formability, good weldability by all common welding processes, it is suitable for machining and has excellent corrosion resistance, even in marine environment. Corrosion resistance can be further improved by anodic oxidation. This alloy is used in engineering, automotive, construction, or hydraulic and pneumatic components. [1]

In Tab. 7 are shown mechanical properties depending on the heat treatment method.

Table 7 - Mechanical properties of alloy EN AW 6082 depending on the heat treatment [6]

	Annealed	Annealed + NA	Annealed + AA
$R_{p0,2}$ [MPa]	max. 110	110	255
R_m [MPa]	max. 160	205	310
$A_5 (A_{10})$ [%]	13 (15)	12 (14)	9 (10)

3 Strengthening mechanisms

Strength is one of the basic characteristics of a material. It is a function of the binding forces, structure and chemical composition of the material. In general, higher strength is found in metals which having a higher melting point.

Aluminum has a relatively low melting point, a relatively high thermal expansion coefficient, and the bonding energy between the aluminum atoms is not great. This results in low strength characteristics. [2] [7] [8]

The strength of the pure metals is very often lower than that required for their application. For this reason, it is necessary to look for ways to increase this strength. For pure metals, strength can be increased by cold forming or by reducing grain size. If a higher strength is required, it is necessary to switch from pure metals to the alloys. Alloy strength can be increased by alloying or heat treatment. It is therefore advisable to combine several methods, such as alloying, forming, grain size control or heat treatment, for optimum properties. [2] [7] [8]

Strengthening of the material can be characterized as an increase in resistance to the occurrence and movement of dislocations. The stress required to effect plastic deformation depends on the type, amount, and distribution of obstacles that prevent dislocation movement. The barriers to movement of dislocations include dislocation networks, grain boundaries and sub-grains, atoms alloying elements or precipitates. The following subchapters describe the impact of individual obstacles on the increment of the strengthening. [2] [7] [8]

3.1 Dislocation hardening

Dislocation hardening is based on the interaction of movable dislocations with embedded dislocations, dislocation clusters and dislocation networks and depends on the amount of dislocations in the material. The number of dislocations is characterized by the density of dislocations. Dislocation density is the total length of dislocation lines in a unit of volume.

$$\rho = \frac{L}{V}$$

Where: ρ is dislocation density, L is total length of dislocation lines, V is crystal volume.

The increment of dislocation hardening can be expressed by relation

$$\Delta\sigma_d = 2\alpha Gb\rho^{\frac{1}{2}}$$

where α is the material coefficient in the range of 0.5 to 1, G is the shear modulus, b is the Burgers vector, ρ is the dislocation density,

Dislocation hardening is related to grain boundary hardening because dislocation is inversely proportional to grain size.

$$\rho = K \cdot d_z^{-1}$$

where ρ is dislocation density, K is constant, d_z is grain size.

For aluminum and its alloys, it should be noted that dislocation hardening is affected by the specific energy of the stacking fault. Aluminum is a metal that has a high energy of stacking fault $\gamma = 2.10^{-5} \text{ J}\cdot\text{m}^{-2}$, with a narrow band of stacking fault. This means that the mobility of dislocations by cross slip is easier than for metals with low energy of stacking fault such as a steel. The resulting hardening will not be as pronounced as for low energy stacking fault. [2] [8]

3.2 Grain boundary hardening

The polycrystalline material is composed of differently oriented grains separated by boundaries. Grain boundaries are an obstacle to the movement of dislocations; The influence of grain boundaries on mechanical properties can be expressed by grain sizes. In general, the smaller the grain, the larger the proportion of boundaries. The finer the grain, the better the strength and plastic properties.

Due to the influence of grain size on yield strength and hence grain boundary strength, the Hall-Petch relationship was derived.

$$R_e = \sigma_0 + K_z \cdot d_z^{-1/2}$$

where R_e is the yield strength, σ_0 is the stress for the movement of dislocations within the grains, K_z expresses the effect of the grain boundary on the induced slip in adjacent grains, d_z is the mean grain size. [2] [8]

Fig. 2 shows the yield strength dependence on the grain size for copper and aluminum. It is apparent from this dependence that the effect of grain size is not as pronounced in the case of aluminum as it is in copper. [9]

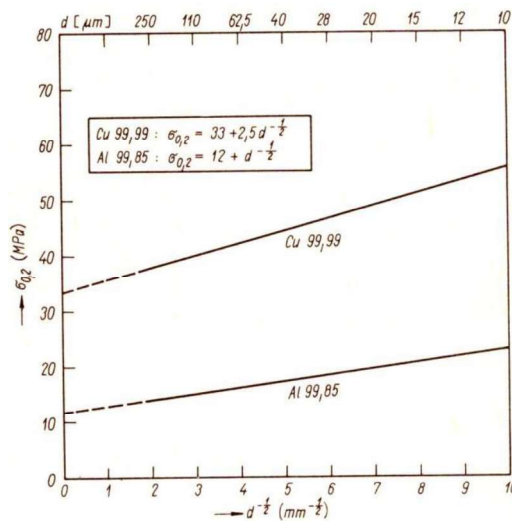


Figure 2 - Dependence of yield strength on the grain size of aluminum and copper [9]

3.3 Hardening by alloying

Strengthening with alloying elements and increasing the yield strength can be obtained if the alloying element atom distorts the basic metal lattice. This means that atoms of other elements act as sources of stress fields in the matrix. Depending on the size of the aluminum radius r_{Al} and the radius of the alloying element r_x , tensile or compressive stresses arise. The interaction of the stress fields of the atoms of the alloying element leads to an increase in the slip stress, in other words an increase in the strength properties. Fig. 3 shows the dependence of the elements on increasing the strength of aluminum.

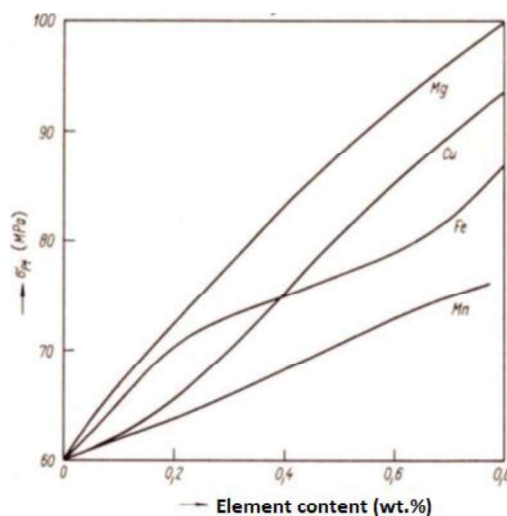


Figure 3 - Influence of element content on the increase of aluminum strength [9]

The Tab. 8 shows the difference in the radius of the alloying element and the aluminum, as well as the increase in yield strength and strength as a function of the concentration of the alloying element. [2] [8] [9]

Table 8 - Influence of alloying elements on substitutional reinforcement of aluminum [1]

Element	$r_X - r_{Al}$ [%]	$R_{p0.2}$ [MPa/Wt%]	R_m [MPa/Wt%]
Si	-3.8	9.2	39.6
Zn	-6	2.9	15.2
Cu	-10.7	13.8	43.1
Mn	-11.3	30.3	53.8
Mg	11.8	18.6	50.3

The increment of alloying hardening can be expressed as follows formula

$$\Delta\sigma_L \approx \sum_j A_j \cdot c_j^m$$

Where A_j is the proportionality constant of the alloying element, c is the concentration of the alloying element, m ranges from 0.5 – 1. [8]

3.4 Precipitation hardening

The precipitates are formed by the decomposition of the supersaturated solid solution. A stress field is created around the precipitate which retards the movement of dislocations. The finer the particles and the smaller their distance, the greater the effect on the reinforcement. Depending on the coherence of the interface between the precipitates and the matrix, the dislocation interaction proceeds according to either the Friedel or Orowan mechanism. Fig. 4 shows dependence of stress for dislocation passage on particle size. The critical particle size corresponds to the maximum strength increase, and as the particles grow further, the strength decreases. [2] [8]

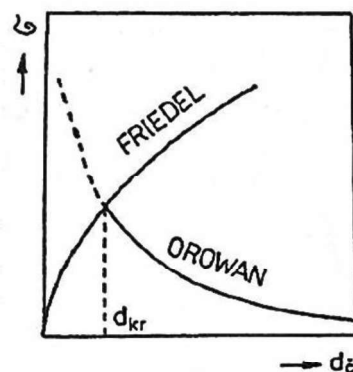


Figure 4 - Stress for the passage of the dislocation through the particle depending on the particle diameter [8]

The Friedel mechanism assumes that the particles have a coherent or semi-coherent interface. The particles are small, and the dislocation passes through the particle. Fig. 5 shows the passage and intersection of a particle by dislocations. [2] [8]

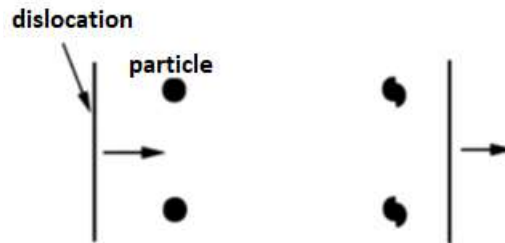


Figure 5 - Friedel mechanism [7]

For coherent and semi coherent particles, the stress relation for dislocation passage applies

$$\tau_{kr} = \tau_m + 2G\delta_c$$

where τ_{kr} is the critical stress, τ_m is the slip stress of the base matrix, G is the shear modulus, δ_c the lattice mismatch parameter.

$$\delta_c = \frac{a' - a}{a}$$

where a' is the lattice parameter of the particle, a is the lattice parameter of the base matrix.

The Orowan mechanism applies when the particles reach a critical and larger size, an incoherent interface is created, and the dislocations no longer pass through the particles but bypass them. Fig. 6 shows extrusion of dislocation through particles to form dislocation loops.

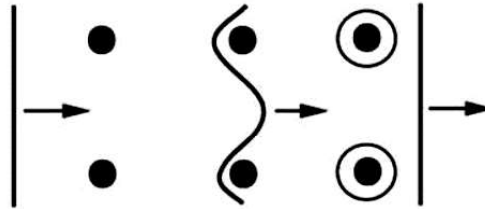


Figure 6 - Orowan mechanism [7]

For non-coherent particles, the stress relation applies to the movement of dislocation across the particles.

$$\tau_{kr} = \tau_m + \frac{2Gb}{\lambda}$$

where τ_{kr} is the critical stress, τ_m is the slip stress of the basic matrix, G is the Shear modulus, b is the Burgers vector, λ is the interparticle distance. [2]
[8]

4 Recovery and recrystallization

During the deformation of metals, a part of the deformation energy is absorbed. This energy is called stored energy. The stored energy causes the growth of internal energy and therefore the metal gets into an unbalanced metastable state.

During subsequent heating, the metal tendencies to return to equilibrium state before deformation. The stored energy is re-released and is the driving force of the relieving processes. The deblocking processes are divided into a two processes, recovery and recrystallization.

Recovery is characterized by the elimination of redundant point disturbances to the equilibrium concentration and a partial reduction in the density of dislocations and their arrangement in the energy-favorable state.

Recrystallization is characterized by the formation of new grains in the original deformed structure with a significant reduction in dislocation density and a significant change in mechanical properties.

Depending on the deformation temperature, the hardening and softening processes are further divided into static and dynamic. Static processes take place during the heating of the cold-formed metal. Dynamic processes take place during hot forming and at the same time hardening and softening processes. In addition to dynamic recrystallization and recovery that take place directly during deformation, the structure is also affected by post dynamic recovery and recrystallization that occurs immediately after deformation and static recrystallization and recovery, which begins to appear a few seconds after the deformation. [8] [10] [11]

Fig. 7 shows the course of the structural changes during recovery and recrystallization and the change of properties during a softening. [12]

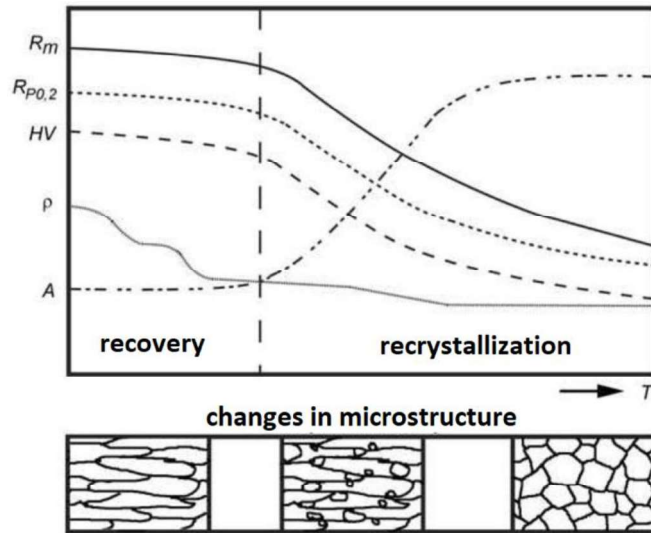


Figure 7 - Change of selected mechanical properties depending on temperature [12]

It can be seen from Fig. 7 that the physical properties and the slight mechanical properties change during the recovery. Recrystallization significantly influences mechanical properties. [8] [12]

4.1 Recovery

Recovery takes place in the temperature range of 0.25 to 0.30 T_M . During the recovery, the deformation structure is maintained, and new undeformed grains are not formed. During the recovery, sub structural changes occur, decrease of concentration of point defects, dislocation density decreases and their arrangement changes.

The first phase of recovery is the recovery of point defects. The second and most important phase is polygonization, which may not always occur. [2] [8] [11]

4.1.1 Recovery of point defects

Reducing the excess concentration of point defects during annealing back to equilibrium concentration is accomplished by thermally activated migration of defects to burrows and their disappearance. The rate of recovery of point failures during annealing can be described by relation

$$-\frac{dc}{dt} = K_0 \exp\left(-\frac{\Delta H}{RT}\right) C^\alpha$$

where c is the point defects concentration, t is the annealing time of reaching the concentration c , K_0 is the temperature and concentration independent constant, is the activation enthalpy, ΔH is activation enthalpy, R is gas constant, T the temperature, α is the order of recovery kinetics. [2] [8] [11]

4.1.2 Polygonization

During polygonization, part of the dislocations abolished and their arrangement changes. Part of the dislocations of the same sign are arranged in the dislocation walls and thus assume stable positions. By arrangement in the dislocation walls, sub-grains are formed separated by low-angle boundaries. Taking stable positions reduces the stored energy and eliminates the curvature of the lattice. Fig. 8 shows the process of polygonization. [2] [8] [10] [11]

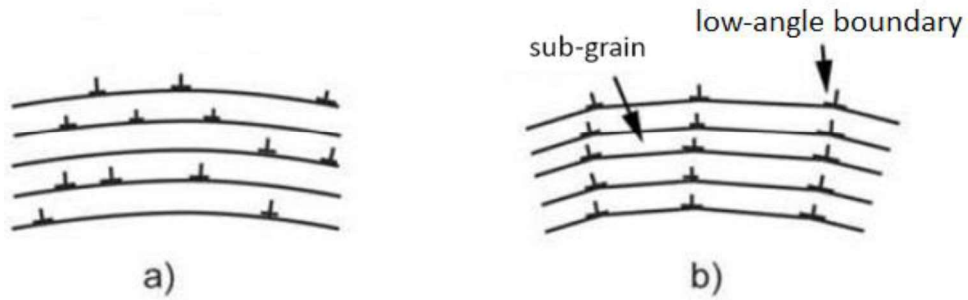


Figure 8 - Schematic representation of polygonization a) deformed stage, b) recovered substructure [8]

The application of polygonization is influenced by the energy of the stacking fault. For aluminum, which has high stratification stacking fault energy, rearrangement of dislocations is easier, and therefore polygonization is more effective. The share of energy released in the recovery phase can be up to 40%. [2] [8]

5 Recrystallization

Recrystallization takes place in the temperature range of 0.35 to 0.45 T_M . During recrystallization, new polyedric grains with a low concentration of imperfections are formed from the deformed grains. Recrystallization releases the rest of the stored energy. Recrystallization is a process in which high-angle grain boundaries move. Wide angle boundaries range from lower dislocation density sites to higher dislocation density sites. The movement of high-angle boundaries leads to the “sweeping” of dislocations, which means that dislocations integrate into moving boundaries. The dislocation density gradually decreases to the value that was in the metal before plastic deformation. These processes are accompanied by a significant decrease in strength and hardness, an increase in ductility and toughness. [2] [8] [10] [11]

5.1 Mechanism and kinetics of recrystallization

Recrystallization is usually divided into primary recrystallization, grain growth and subsequent processes, which are called secondary or tertiary recrystallization.

5.1.1 Primary recrystallization

Most often it occurs by the formation and growth of recrystallizing nucleuses of the same crystalline lattice. After very small plastic deformations, no new nucleuses are formed, and the recrystallization is affected by migration of the original high-angle grain boundaries or parts thereof. Both cases are discontinuous recrystallization.

There is also a discontinuous primary recrystallization where the consolidation processes take place simultaneously throughout the sample volume. This occurs when the braking forces due to precipitation and segregation exceed the driving force of recrystallization. The stiffening process is controlled by the formation and distribution of the precipitate and no high-grain boundaries migrate.

Classical discontinuous primary recrystallization is divided into two phases, nucleation and grain growth. It lasts until the deformed structure is replaced by growing grains, the grains touching each other.

There are several classical models for the process of the nucleus's formation of new recrystallized grains. The most commonly used models include the model of sub-grain growth by migration of their boundaries, the model of merging

of sub-grains and the model of deformation-conditioned migration of grain boundaries.

The model of nucleation of new grains by sub grain growth by border migration assumes that the nuclei are based on small deformation-free polygonal sub grains. The low-angle boundary moves and gradually turns into a high-angle boundary. The resulting formation becomes the nucleuses.

The model of coalescence of sub grains assumes that sub grains begin to combine by gradually breaking down the low-angle boundaries between them, while aligning the original mutual disorientation, by rotating the sub grains. This process is completed by the creation and growth of the external high-angle boundary. A recrystallization nucleus is formed.

The model for the formation of nucleuses in low-deformed polycrystalline metals is based on the notion of migration of a part of the original boundary that deflects in the form of a spherical cap Fig. 9. The driving force of the spherical cap migration is the energy proportional to the difference of dislocation densities on both sides of the border. Multiple sub-grains may be involved in the process. [2] [8] [10] [11]

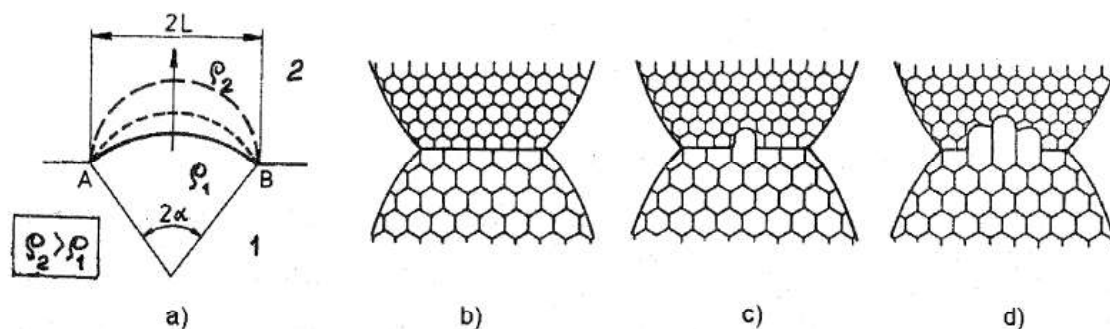


Figure 9 - Scheme of deformation-induced deflection of the original grain boundary [8]

It is now believed that new grains during recrystallization grow from either small volume of recovered sub-grains or sub-structural grains with low dislocation density, which are always present in the deformed structure. These formations become nucleuses and begin to grow when they acquire the necessary disorientation and size. Nucleation is retarded by foreign atoms in solid solution and fine particles.

The nuclei growth phase is followed by the grain growth phase. However, the separation of the two phases is very difficult. If the growth of all grains is uniform, the completion of the primary recrystallization is considered to have reached the structure with recrystallized grains of average size in tens of μm .

After the primary recrystallization phase, the grain coarse phase begins. The driving force of the process is the reduction of total grain boundary energy. There is also, the braking effect of foreign atoms, especially impurities, which are excreted at the grain boundaries, is apparent.

For the evaluation of recrystallization, the total kinetics of the recrystallization, which can be expressed by the Avrami phenomenological equation

$$X = 1 - \exp[-kt^n]$$

where X is the fraction of transformation, t is function of time, k and n are time-independent constants for the particular reaction. The temperature dependence of the coefficient X can be expressed by the relation

$$X = X_0 \cdot \exp\left[\frac{-H_R}{RT}\right]$$

Where X_0 is the temperature independent constant, H_R is the activation enthalpy of recrystallization, R gas constant, T temperature.

After double logging and adjustment, we obtain the dependence of the recrystallized fraction on time, expressed by lines with the slope of the exponent n.

$$\log \ln \frac{1}{1 - X_v} = \log k + n \log t$$

Which is in the called Avrami coordinates $\log \ln \frac{1}{1 - X_v}$ versus $\log t$ the equation of the line whose slope is the kinetic exponent n.

Fig. 10 shows the theoretical curves of the recrystallization curve. Real recrystallization curves cannot be described with just one straight line, but more breaks occur with decreasing n values. It was assumed that the grain boundary migration rate was constant during recrystallization and its mechanism did not change. In fact, however, the rate of migration is declining, and the mechanism is also unchanged. At the final stage of the process, nucleation ceases and the recrystallization is completed by the nucleation-free mechanisms, by the ingrowth of the recrystallized grains into the remnants of the extruded matrix.
[2] [8] [10] [11]

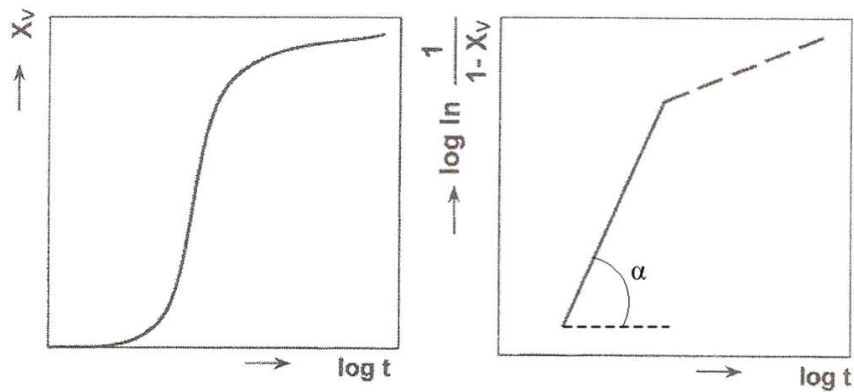


Figure 10 - Theoretical curves of recrystallization kinetics [8]

5.1.2 Secondary recrystallization

This process does not always occur and is characterized by the growth of some grains at the expense of neighbors. This results in local grain coarsening. The start of secondary recrystallization is very slow. Grains that grow at the expense of adjacent grains are larger than the surrounding grains, having a significantly different orientation from both the surrounding grains and the texture of the matrix. Significant growth of these grains occurs by inhibiting the growth of other grains by particles of another phase deposited at their boundaries, or by the presence of a distinctive primary recrystallization texture. The secondary recrystallization temperature is specific to each material. The driving force of secondary recrystallization is about two-digit places smaller than that of primary recrystallization and corresponds to the energy of grain boundary migration at primary grain growth.

For very thin sheets, extraordinary grain growth can occur, the enlargement of which is associated with an increase in the free surface. This process is called tertiary recrystallization. [2] [8] [10] [11]

5.2 Factors affecting recrystallization

5.2.1 Material and its purity

An important material factor is the stratification stacking fault energy. Aluminum has high stratification stacking fault energy and due to the easy movement of dislocations, polygonization is markedly applied.

Foreign atoms in the crystalline lattice of the basic metal slow down recrystallization. At the same temperature, the presence of impurities causes an increase in the recrystallization time and an increase in the recrystallization start temperature. Trace number of foreign elements have the highest braking effect.

As the amount of element increases, the effect on recrystallization is less or none. This means that up to a certain concentration of the element the element has a braking effect and at a higher concentration the element does not appear.

The influence of individual elements in the crystal lattice is different. In aluminum, the iron atoms retard the recrystallization more than in the same amount of copper or silicon. The elements with the lowest solubility in the solid solution most increase the recrystallization temperature. [2] [8] [10] [11]

5.2.2 Influence of precipitation and grain size

In hardened alloys, recrystallization is affected by the precipitates. It depends on the size, amount and whether precipitation occurs before, during or after recrystallization. The precipitated particles can either retard or accelerate the recrystallization. Small particles retard recrystallization (prevent grain boundary migration), coarse particles accelerate it (local increase in the intensity of a stress).

The course of recrystallization depends on the precipitation temperature. It is necessary to know the temperature dependence of the beginning of the recrystallization and precipitation. Fig. 11 is a graphical representation of the time of onset of recrystallization t_R and the start of precipitation t_P at c_0 concentration.

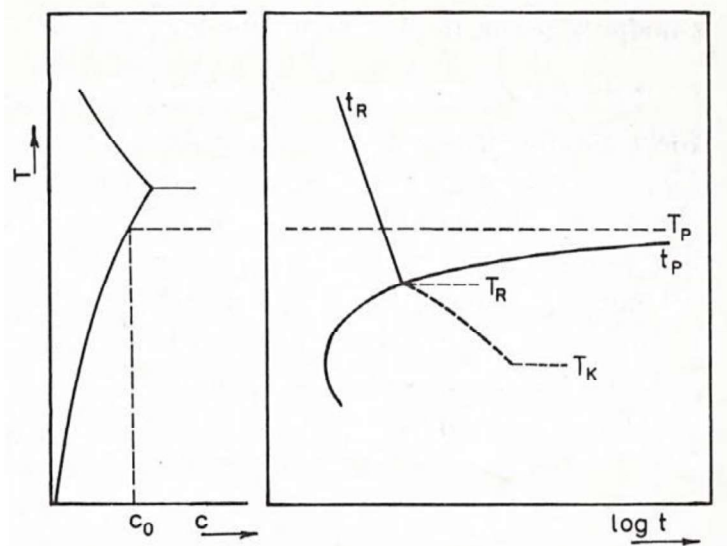


Figure 11 - Progression of recrystallization start t_R and start of precipitation t_P for alloy with concentration c_0 [9]

The temperature T_R indicates a case in which both processes start simultaneously and interact with the entire material volume. If the temperature is lower ($T < T_R$), recrystallization is affected by the secondary phase particles.

If the temperature is higher ($T > T_R$), precipitation occurs in a partially or fully recrystallized structure.

Grain boundaries are the preferred site of nucleation of the recrystallization nuclei. With the same deformation of the finer grain structure, more strain energy is stored, thereby increasing the driving force of the recrystallization. [2] [8] [10] [11]

5.2.3 Extent of deformation

During the recrystallization under small deformation (10-15%) the grains are growing usually rapidly, which is accompanied by a deterioration of the mechanical properties. Small deformations are characterized by high inhomogeneity of deformation, low driving force of recrystallization and grain coarsening after recrystallization. At deformations up to 90% the kinetic values increase with increasing degree of deformation due to stored energy. Recrystallization thus accelerates with increasing deformation. [2] [8]

5.2.4 Temperature of deformation

Depending on the deformation temperature, the hardening processes are further divided into static and dynamic. Static processes take place during the heating of the cold-formed metal. The dynamic processes take place during hot forming and the hardening and unhardening processes take place simultaneously. These processes are divided into dynamic recovery and dynamic recrystallization. [2] [8]

5.2.5 Dynamic recrystallization and recovery

As the deformation temperature increases, the mutual proportion of the deformation mechanisms changes and from a certain temperature also the restoration processes, whose intensity increases with temperature, start to apply. The restoration process can only take place partially or completely dynamically, during deformation. Dynamic restoration can be divided into dynamic recovery and dynamic recrystallization.

Dynamic recovery is the result of simultaneous strengthening and restoration processes. It cannot be conceived of as a combination of previous deformation and subsequent static recovery. The driving force is the internal stress supplemented by the external stress. The main mechanism is transverse slip. For this reason, dynamic recovery is preferentially applied to high-energy metal stacking fault.

Dynamic recovery produces sub-grains whose size and mutual disorientation depend on the material, temperature and strain rate. The size of the sub grains can be described by relation

$$d_s^{-1} = a + b \log Z$$

a,b are constants, Z is a Zener-Hollomon parameter to evaluate the effect of temperature and strain rate.

$$Z = \dot{\varepsilon} \cdot \exp \frac{\Delta H}{RT}$$

where $\dot{\varepsilon}$ is strain rate, ΔH is activation enthalpy, R is gas constant, T is temperature.

This parameter includes the effect of temperature and strain rate and the boundary between dynamics recrystallization and recovery. Dynamically recovered grains are larger than those after static recovery.

The dynamically recrystallized structure is the result of parallel strengthening and restoration processes. Stacking fault are preferred for low energy metals, in other words materials where dynamic recovery is not significantly applied. The difference from static recrystallization is in the kinetics of nucleation and subsequent growth of the recrystallization grain. The size of the dynamically recrystallized grains is not limited by the contact of adjacent grains. Due to the simultaneous deformation, the density of dislocations increases, thereby reducing the driving force of recrystallization. The size of the original grain does not affect the size of dynamically recrystallized grains, it only affects its ratio. The temperature and degree of deformation required for dynamic recrystallization are higher than for static recrystallization. Dynamically recrystallized grains are slightly elongated in the direction of deformation compared to static grains and show increased dislocations density. [2] [8] [10] [11]

6 Plastic deformation

Due to external forces the loaded specimen changes their shape. A change in specimen shape is called deformation. Specimen deformation can be divided into elastic and plastic. The elastic deformation is reversible, that is, after relieving the body, it returns to its original shape. Elastic deformation is expressed by Hook's law, where the deformation is directly proportional to the stress, up to the yield point.

If the load is higher than the yield strength, Hook's law ceases to apply and the relationship between stress and strain ceases to be linear. After relieving deformation does not disappear and causes a permanent change in the shape of the specimen. This change of specimen shape is called plastic deformation. [2] [8]

6.1 Plastic deformation and its mechanisms

Plastic deformation always occurs by movement of dislocations. The basic mechanism of plastic deformation is slip, the complementary mechanism is twinning. Twinning is applied at high strain rates and low temperatures. At elevated temperatures other mechanisms such as grain boundary slips, diffusion and dislocation creep apply. Fig. 12 shows the difference between slip and twinning mechanism [8]

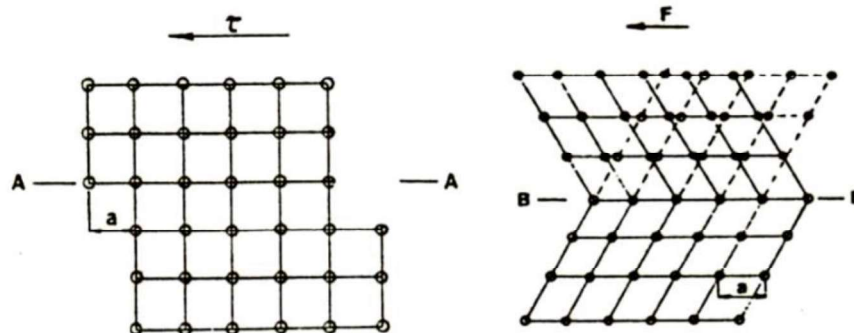


Figure 12 - Slip deformation on the left, twin deformation on the right [8]

6.2 Slip mechanism

The slip runs in the slip planes and slip directions, which together form the slip system. The slip preferably takes place in the planes and directions most densely occupied by the atoms. For body-centered cubic lattices, are planes $\{110\}$, $\{112\}$ and directions $\langle 111 \rangle$, for face-centered cubic lattices, are planes $\{111\}$ $\langle 110 \rangle$, for hexagonal lattices, is the base plane $\{0001\}$ with the direction $\langle 1120 \rangle$.

The slip is realized by moving dislocations in the slip plane of the dislocations in which the shear stress is greater than the critical slip stress. The dimension of the critical slip stress depends on the type of metal, cleanliness and condition, as well as the stress conditions. More slip systems, with a cubic grating of at least five, increment on larger deformations of the polycrystalline material, depending on the orientation, dimension of the force and deformation conditions. Deformation conditions include temperature, dimension and rate of deformation. Aluminum, like silver, gold or nickel, has a face-centered cubic lattice that has 12 slide systems. [2] [8] [13]

6.3 Twinning mechanism

Twinning is a deformation mechanism effected by the passage of partial dislocations through the crystal. Partial dislocation is characterized by a Burgers vector that is smaller than the translational lattice vector. In twinning, a segment of the crystal lattice is shifted to make a mirror image of the non-moved segment of the lattice. Atoms are displaced only by fractions of interatomic distance. Twinning usually occurs in a series of parallel slip planes. Since the critical twin stress value is higher than the critical slip stress value, slip deformation is preferable, twinning is used as a complementary deformation mechanism where there are not enough slip systems. For metals that have high stacking fault energy, twins are usually not formed. Twinning is proceed by low deformation temperature and high strain rate. [2] [8] [13]

6.4 Deformation energy

During plastic deformation a part of the deformation energy is absorbed in the metal and thus the internal energy increases. This change in internal energy is called stored energy. The stored energy is released during the annealing and serves as a driving force of the disengagement mechanisms. The change in internal energy by plastic deformation is influenced by the formation of crystal lattice defects, mainly by dislocation. The stored energy is released whole or in part during the recrystallization and recovery processes. The factor that affects the stored energy of the deformed metal is the stacking fault energy. [2] [8] [13]

6.5 Deformation structure

During plastic deformation, some of the grains rotate in the direction of deformation. As the deformation increases, the grain orientation is parallel to the forming direction, and the grain lengthens in this direction, even with deformable particles and phases in the material. Since the individual grains are differently oriented, there is a different plastic deformation in the individual grains and thus different reinforcement. Fig. 13 shows how the structure is deformed from an equiaxed grain arrangement.

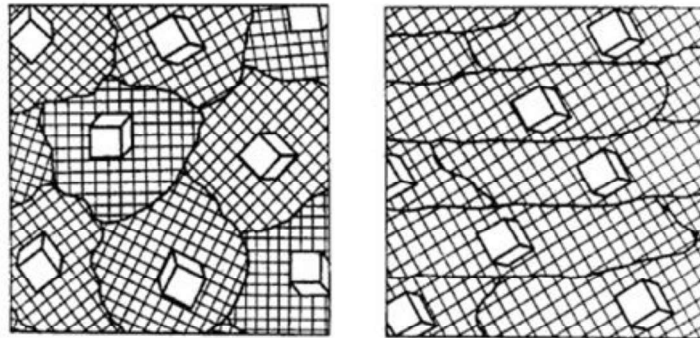


Figure 13 - Representation of deformation structure formation [13]

We can divide the methods of aluminum forging into two categories, hammer forging and die forging. In the hammer forging, repeated blows are applied only to a portion of the surface of the material, while the die forging causes one or more blows to apply to all or almost the entire outer surface of the workpiece. [2] [8] [13]

6.6 Homogeneity of deformation

The final properties of forgings are influenced by all technological operations during production. Especially in the case of hardened alloys, a significant inhomogeneity and anisotropy of the structure and properties must be taken into account, as in the case of compacts. In forgings the material flow varies in different parts of the cross-section, which complicates the evaluation of properties. Therefore, it is usually necessary to precisely define the sampling points, considering how the forging will be stressed and where its critical point is.

In semi-finished products made of cast material, the most important for its resulting properties is the removal of the casting structure by sufficient deformation. If the forging is followed by die forging, there is no risk of insufficient deformation.

In the case of free forging, it is necessary to include inter-operative annealing to restore the deformation ability. In these cases, it is necessary to select the forming process that prevent grown of zones with a critical amount of deformation, which leads to local coarsening of the structure.

Coarse-grained recrystallized layers are a common problem in die forgings. These layers are usually on the forging surface and are formed by long elongated grains in the direction of the material flow. These areas have lower mechanical properties, fatigue properties and corrosion resistance. [1] [2]

6.7 Influence of temperature on plastic deformation

Plasticity is the ability of a material to plastically deform to the extent of exceeding the yield point until failure of the material. On the other hand, formability is much more useful. Formability is the ability of a body to deform plastically under certain forming conditions. The formability depends on the plasticity of the material, the geometry of the molded body and the forming conditions. [2]

6.8 Deformation resistance

The term deformation resistance is used instead of the critical contractual stress in describing the forming. The deformation resistance is an internal stress that arises as a reaction against external forming forces. The internal stress shall be such as to cause plastic deformation. The deformation resistance depends on the temperature, strain rate, dimension of deformation and influence of deformation strengthening. [2]

7 Heat treatment of aluminum alloys

There is no fundamental difference between the heat treatment of the alloys for forming and casting; According to ČSN 42 0056, heat treatment of aluminum and its alloys can be defined as: "Process in which a product or part thereof is subjected to one or more annealing cycles in order to achieve the desired structure/substructure and properties" [14]

Heat treatment of aluminum can be divided into two groups:

- Annealing
- Solution heat treatment

7.1 Annealing

Annealing is a kind of heat treatment aimed at obtaining a state of material that is close to equilibrium. The annealing process is shown in Fig. 14. It shows the dependence of the product temperature on time.

The annealing process consists of three parts - heating, soaking and cooling. The course of annealing depends mainly on the chemical composition of the alloy and the type of annealing.

Heating is a process in which the temperature of the product is raised to the annealing temperature. The heating rate is characterized by a rise in temperature versus time.

Soaking is a process that takes place at the desired annealing temperature for the time required to make the desired changes to the product material.

Cooling is a process in which the temperature of the product is reduced from the annealing temperature. The cooling rate is characterized by a decrease in temperature versus time. [1] [2]

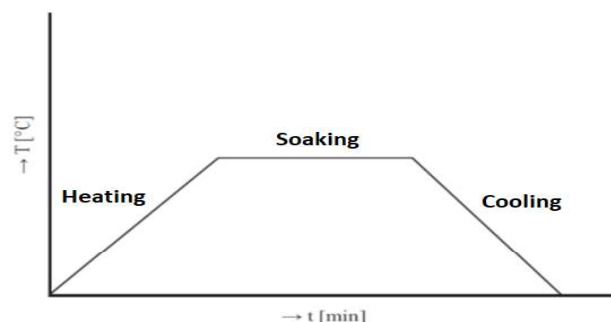


Figure 14 – The annealing process [1]

7.2 Solution heat treatment

Solution heat treatment is a heat treatment that is used to obtain high strength properties of aluminum alloys. The aim of this heat treatment is to eliminate fine precipitates in the base metal matrix. The basic preconditions for an alloy to be curable are:

The alloy must contain sufficient alloying element (s).

The alloying element (s) must have sufficient solubility in alpha solid solution.

The solubility of the alloying element (s) must increase in alpha solid solution with increasing temperature.

The mechanical, physical and technological properties of alloys can be changed to a considerable extent by solution heat treatment. The condition is that these alloys have a significant change in the solubility of the alloying element at temperature in terms of the respective equilibrium diagram. This process consists of two parts - solution annealing and aging. [1] [2]

7.2.1 Solution annealing

Solution annealing is heating to a dissolving temperature, soaking at that temperature for a time that is required to convert one or more of the intermetallic phases into a solid solution, and then cooling at a supercritical rate necessary to obtain a supersaturated solid solution. The critical rate is the lowest possible cooling rate at which the supersaturated solid solution does not decompose. [1] [2]

7.2.2 Aging

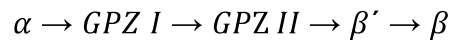
It can be done at room temperature - natural aging, or at elevated temperature - artificial aging. For technological reasons, may be used gradual aging. During aging, the subculture changes and with it the physical technological and mechanical properties change. [1] [2]

7.2.2.1. Artificial aging

In Al-Mg-Si alloys, the release of the supersaturated solid solution is achieved only by artificial aging. These alloys are sensitive to the delay between cooling from solution annealing temperature and the start of artificial aging to achieve maximum strength properties. One possibility is to perform artificial aging

immediately after cooling from the solution annealing temperature, and the other is to perform them after a longer period. [1]

In Al-Mg-Si alloys, the supersaturated solid solution release as follows.



where α is a supersaturated solid solution, GPZ I is disorganized needle-shaped zones, GPZ II is ordered needle-shaped zones, β' is an intermediate semi-coherent phase, β is an equilibrium non-coherent Mg_2Si phase.

EXPERIMENTAL PART

Forging production is a technologically demanding process whose aim is to achieve the best possible structural characteristics and thus the final properties of the manufactured part. The main parameters are the deformation temperature, the magnitude of the deformation, the number of deformation cycles, the rate of deformation and also the method of cooling. Very important in this case is the semi-finished product, whose structure is influenced and significantly changed by forming. The aim of this work is to evaluate the influence of deformation parameters on the resulting structure and mechanical properties. The semi-finished products are round bars manufactured by horizontal continuous casting or by extrusion. A 48 metallographic samples were produced from 24 semi-finished products. Due to its extent, the experimental part was divided among more students. My colleagues, who cooperated on the experiment, were Ing. Tom Procházka (already graduated) and Veronika Kozáková.

8 Samples preparation

8.1 Input parameters of semi-finished products

Input parameters of semi-finished products for the processing of test samples are given in Tab. 9.

Table 9 – Input parameters of the semi-finished products

Diameter	50 mm
Length	100 mm
Material	EN AW 6082
Production technology	HCM/EXT
Heat treatment	From production

8.1.1 HCM

This technology is used only for large-scale production. The producing smaller, thin-walled and structurally complex castings with exact dimensions and excellent surface quality are produced. It is mainly used for non-ferrous metal alloys with medium casting temperatures (aluminum, zinc, magnesium). It is mainly used in the automotive and aerospace industries.

Characteristic of this manufacturing process is the filling of the mold cavity, with a melt at a temperature lower than the liquidus temperature, through an inflow system with very small cross sections at high speed. For aluminum alloy castings, cold chamber pressing machines are used.

8.1.2 Extrusion

Together with rolling it is the most used method of forming aluminum alloys. Advantages of extrusion include the production of different types of extrusions in a small number of operations with a simple or complex cross-section. Furthermore, high accuracy, high-quality surface is achieved and a quick change of product range is possible. The disadvantages of this technology are the inability to mold the entire material volume and the short tool life of the dies. Aluminum alloys are very different in hot deformation behavior and therefore one universal method cannot be used.

Pressing takes place on semi-continuously cast round ingots, which have been heated to the required temperature at which no cracks are formed yet. Then the ingot is inserted into the press, which was also heated to a predetermined temperature. Subsequently, the punch pushes the ingot through the die. [3] [11]

8.2 Free forging of the samples

The experimental process was designed and built with respect to the similarities with the actual course of the forming operations and the heat treatment of the alloys. The aim was to achieve partial states into which the semi-finished product reaches during its processing. At the same time to map the processes leading to the final properties of the finished product.

8.3 The variants of the free forging

Free forging was running by compressing a cylinder laid between horizontal anvils. A deformation of 50 mm diameter is defined according to the desired upset height as the ratio of upset height to the original dimension. The relation for the calculation is expressed as

$$\varepsilon_h = \frac{h_0 - h_1}{h_0} \cdot 100 [\%]$$

where h_0 is the original diameter and h_1 is the height after the first deformation. For a modified relationship then applies to repeated deformation

$$\varepsilon_{ho} = \frac{h_0 - h_1}{h_0} + \frac{h_1 - h_2}{h_0} \cdot 100 [\%]$$

where h_0 is the original diameter, h_1 is the height after the first deformation and h_2 is the height after the second deformation.

Samples for the experiment were made from semi-finished products deformed according to the following parameters that are shown in Tab. 10.

Table 10 – Parameters of deformation

1st deformation [%]	Height after 1st deformation	2nd deformation [%]	Height after 2nd deformation	Total deformation	Designation
0	50	0	50	0	0
20	40	0	40	20	2
40	30	0	30	40	4
70	15	0	15	70	7
20	40	40	20	60	24
40	30	20	20	60	42

8.4 The parameters of free forging

The blanks were placed in an oven and heated to a forging temperature of 550 °C. A free forging tool with a horizontal anvil was clamped. The tool was heated to working temperature 160 °C.

After the heated to a temperature of 550 °C, the semi-finished products were put between straight anvils. Hardened steel plates were inserted between the anvils to achieve the desired upset height.

The repeat deformed specimens were cooled in air after its first deformation, then reheated and forged to the desired height. After the forging process, the samples were cooled in air. After the cooled down, half of the samples were heat treated.

8.5 The parameters of heat treatment

Solution annealing: temperature = 530 °C,

Solution annealing time = 60 minutes

Delay between solution annealing and artificial aging: 24 hours

Artificial aging: Temperature = 170 °C, aging time = 7 hours

9 The evaluation of the macrostructure

The problem of die forgings made of aluminum alloys is the formation of a coarse-grained layer in the area of critical deformations, in the surface layer. Al-Mg-Si alloys, such as EN AW-6082 are susceptible to the formation of coarse-grained surface layers. These layers cannot be removed by heat treatment, on the contrary, the coarse-grained areas can become larger. Areas of the coarse-grained surface layer have lower mechanical, fatigue properties, have lower corrosion resistance and deteriorate the forging surface quality.

The cutting and milling process is followed by an acid pickling process. The acid pickling procedure is as follows: the scratch pattern is first immersed in sodium hydroxide (NaOH), followed by rinsing with water, immersed in nitric acid (HNO₃) and finally rinsing with water.

Observing of the acid pickled semi-finished products was found, that only the semi-finished products produced by the extrusion method exhibit the susceptibility to recrystallized coarse-grained layers, not the semi-finished products produced by the HCM, as it shown in Fig. 15. The recrystallized coarse-grained layer in extruded samples increases with both deformation and heat treatment application.

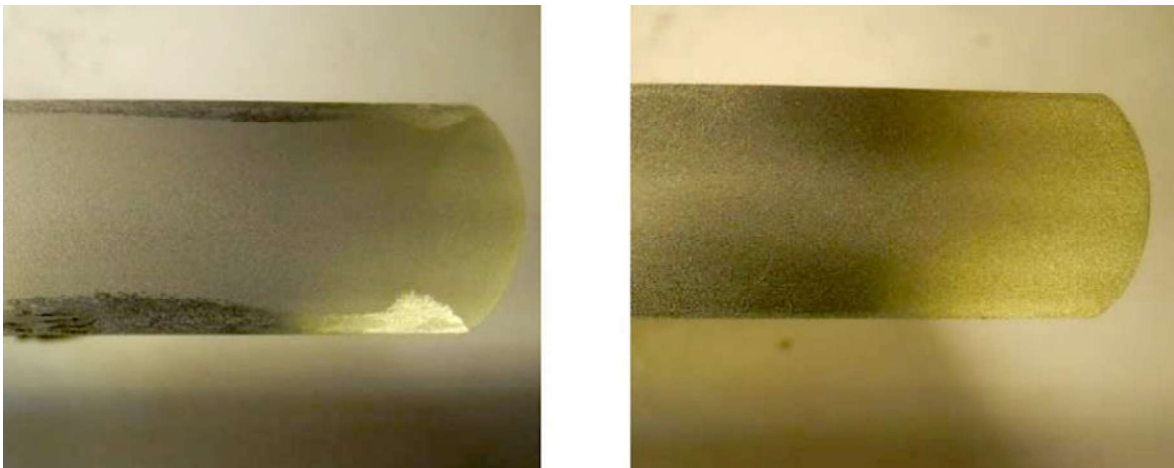


Figure 15 – EXT sample is shown on the left, HCM sample is shown on the right

A more detailed evaluation of macrostructure is included in the thesis of my colleague Tom Procházka.

10 Metallography

The microstructure was evaluated in the cross-section and transection directions in the core area and at the surface of each variant of forged samples.

In order to observe the structure on an optical microscope, it was necessary to prepare a scratch pattern. The scratch pattern preparation process consists of sample separation, pressing, grinding, polishing and etching.

10.1 The cutting of the material

The circular saw LECO MSX255 was used for cutting a samples. The disc 811-077-110 which is designed for cutting non-ferrous metals was used for all the samples. Also, a cutting fluid was used for all samples.

Fig. 16 and 17 show how the preparation of the samples to be pressed was performed. Area A indicates the observation point in the transection, area B indicates the cross section.

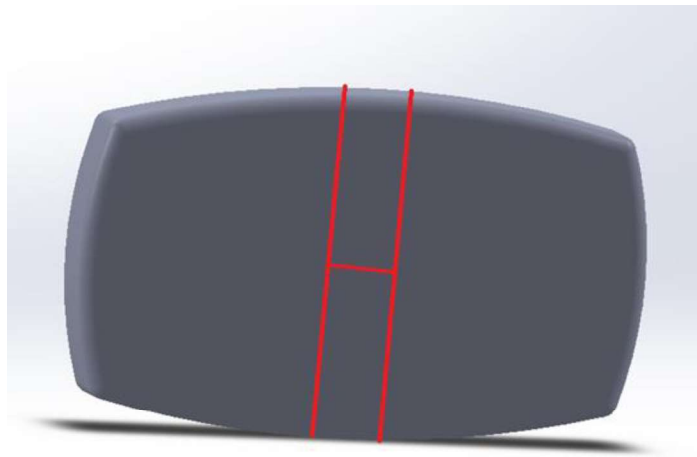


Figure 16 - Scheme of sample preparation procedure

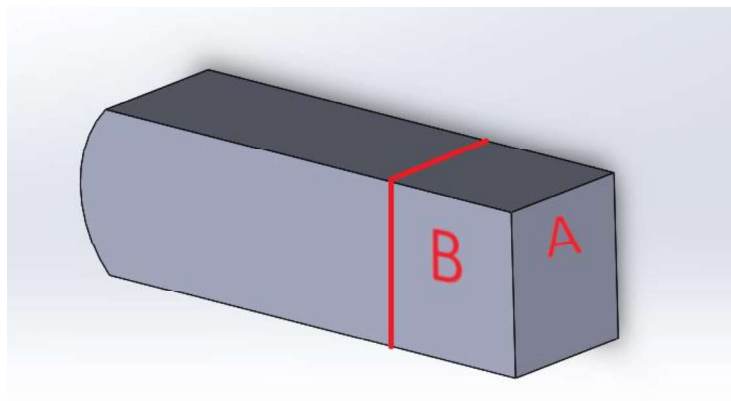


Figure 17 - Area A indicates a transection, Area B indicates a cross section

10.2 The pressing

The samples were pressed into a Bakelite mass using a LECO PR 4X machine.

Pressing parameters: Powder - Black Bakelite Powder, pressing temperature 160 °C, pressing pressure 20 MPa, pressing time - 3,5 minutes. Water cooling to 65 °C.

Subsequently, each sample was described to avoid confusion.

Samples were labeled using a combination of numbers and letters as shown in Fig. 18.

142POX

Figure 18 - Example of the sample naming

The first position denotes the production method of the semi-finished product 1 for extrusion, 2 for HCM.

The second position indicates the deformation of the sample, see Tab. 10.

The third position indicates whether it is a cross section (PR) or transection (PO).

The fourth position denote is used in the case of the heat treatment "X".

10.3 The grinding and polishing

The grinding and polishing of the samples were performed on the LECO GPX 300 machine. The grinding was achieved using abrasive papers from roughness P60 to P4000. Grinding was done manually, the speed of the sanding paper was 200 rpm, the cooling medium was water.

The polishing was carried out in an automatic mode, at a speed of 150 rpm and a pressing force of 24 N. OP-S NonDry was used as the polishing emulsion. Subsequently, the samples were rinsed and dried with hot air.

10.4 The etching

Etching is a very complicated process. To obtain the desired results, multiple etchers with variable etch time had to be used.

Weck's reagent works best for etching to grain boundaries. The composition of the Weck reagent according to [1] is as follows: 100 ml of distilled water, 4 g of potassium permanganate and 1 g of sodium hydroxide. The Weck reagent was in some cases combined with the Dix-Keller reagent. The composition of the Dix - Keller reagent according to [15] is as follows: 190 ml of distilled water and 5 ml of 70% nitric acid.

The etching of the extruded samples was performed with Weck's reagent. The etching time was between 10-30 seconds.

Etching of HCM samples was performed with a combination of Dix – Keller and Weck reagents. The etching procedure was as follows: 10 seconds with Dix-Keller reagent followed by 10-30 seconds with Weck reagent.

11 The tensile test

Among the basic and most widespread mechanical tests is the tensile test. The tensile test is characterized by the predominant uniaxial tensile stress causing elongation of the specimen. The result of this test is usually a tensile diagram Fig. 19 from which basic mechanical characteristics describing material behavior, ultimate tensile strength, yield stress, ductility, area reduction are obtained.

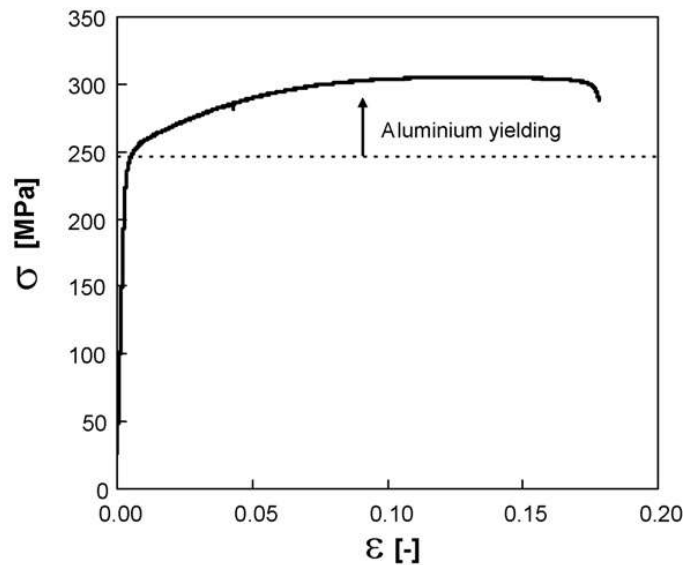


Figure 19 - Stress–strain curve for the 6082-T6 aluminium alloy [16]

The tensile test was performed at ambient temperature according to the valid standard ČSN EN ISO 6892-1 the test was performed on a Zwick testing machine. [17]

Two test specimens were prepared for each variant. Round test specimens with an active part with a diameter of 8 mm and a length of 40 mm were tested, at the ends of which there was an M10 thread for clamping into a testing machine. Samples were made from semi-finished products as shown in Fig. 20.



Figure 20 - Place of sampling for the tensile test

Only the results of the tensile test are given in this work. Veronika Kozáková, with whom we cooperated during the testing, is devoted to detailed processing of these results in her bachelor thesis. The results are shown in Tab. 11.

Table 11 – Results of the tensile test

	R _{p0.2} [MPa]		R _m [MPa]		A [%]		Z [%]	
	EXT	HCM	EXT	HCM	EXT	HCM	EXT	HCM
0	261	146	371	261	18	23	35	44
2	-	115	-	194	-	18	-	49
4	109	113	206	190	16	18	34	49
24	109	113	187	190	18	22	37	47
42	117	119	199	196	18	20	36	52
7	113	144	199	199	18	19	40	53
0X	374	358	408	358	11	16	36	34
2X	348	363	407	363	13	12	36	34
4X	365	366	401	366	13	13	34	38
24X	360	371	396	371	13	13	38	44
42X	327	365	392	365	12	14	37	40
7x	341	361	364	361	12	16	40	49

The results of the tensile stress tests are shown in Fig. 21 to 23.

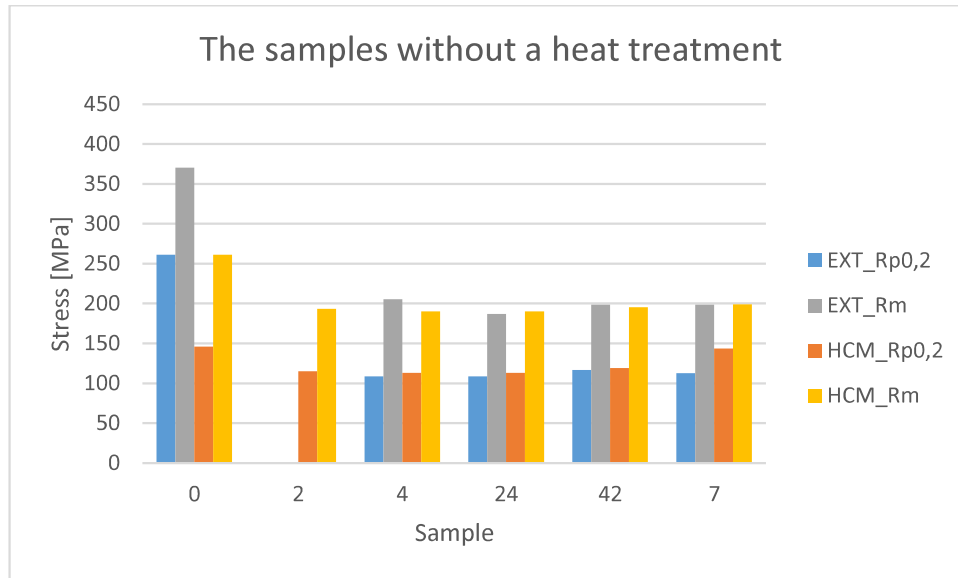


Figure 21 - Values of yield and ultimate strength for samples without heat treatment

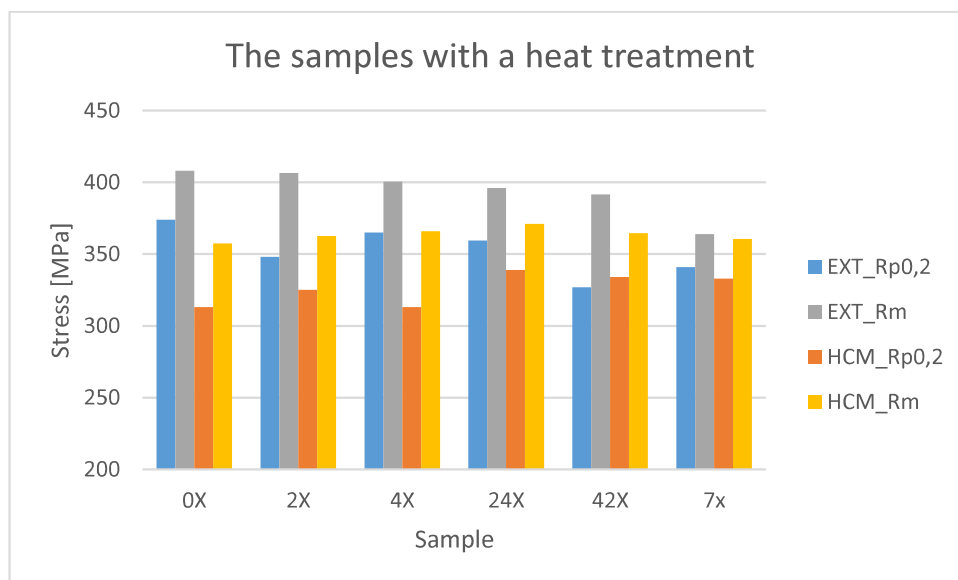


Figure 22 - Values of yield and ultimate strength for samples with heat treatment

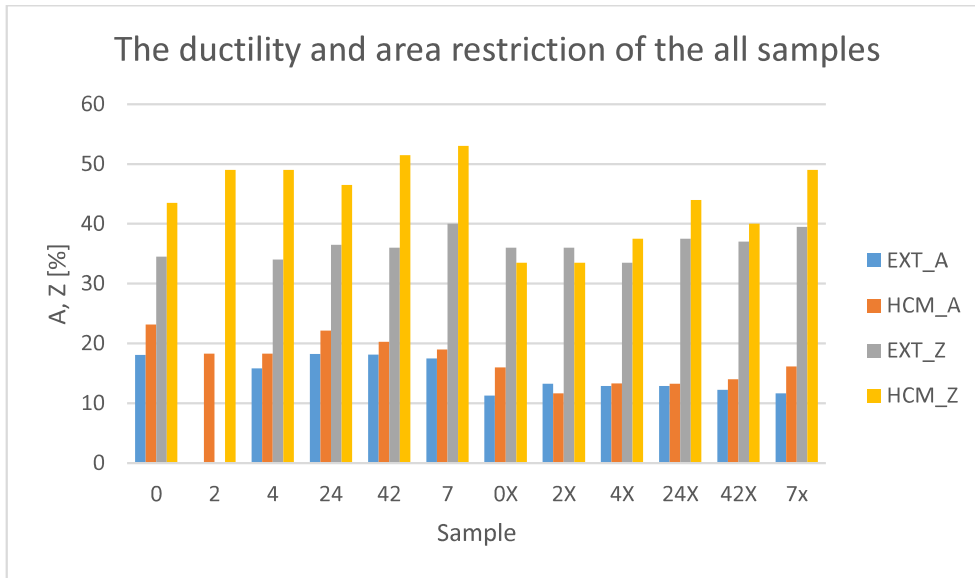


Figure 23 - Values of ductility and area restriction for all the samples

It can be seen from Fig. 21 that the highest values of yield strength and ultimate strength, of the samples without heat treatment, were measured on the semi-finished products without any deformation - on the supplied semi-finished products from a production. Subsequent heating to the forging temperature and deformation reduces the yield strength and ultimate strength. The R_m and $R_{p0,2}$ values are then almost unchanged for all deformation and semi-finished product variants. The only visible growth was measured for the HCM sample with a deformation 70%, where the yield strength was increased.

It can be observed from Fig. 22 that in the heat-treated samples, the yield strength and the ultimate strength of both semi-finished products are equalized with increasing degree of deformation. With a 70% deformation, these values are almost at the same level.

It can be seen from Fig. 23 that in non-heat-treated samples, HCM semi-finished products achieve significantly higher area reduction and ductility values than extruded semi-finished products. For heat treated samples, the ductility of extruded samples slightly decreases with deformation, while for HCM samples it increases. The area reduction of HCM samples increases significantly with the deformation.

12 The evaluation of the microstructure

The aim of the microstructure evaluation was to get an idea of the course of the hardening processes in forged samples and to evaluate the structures in dependence on deformation. The microstructure was evaluated in the surface and core area of the samples.

12.1 The light microscopy

In light microscopy, visible light is used to create contrast. Due to the wavelength of visible light, the resolution of light microscopes is around 0.2 μm .

The aim of the microstructure evaluation on a light microscope was to get an idea of how the structure changes according to deformation and heat treatment. And compare it with the second semi-finished production technique. The microstructure was studied in the surface and core area of forged samples.

Fig. 24 to 29 show how the surface layer has developed for both heat-treated semi-finished products in dependence on deformation.

Fig. 30 to 35 show how the core of the both semi-finished products evolved in dependence on the deformation.

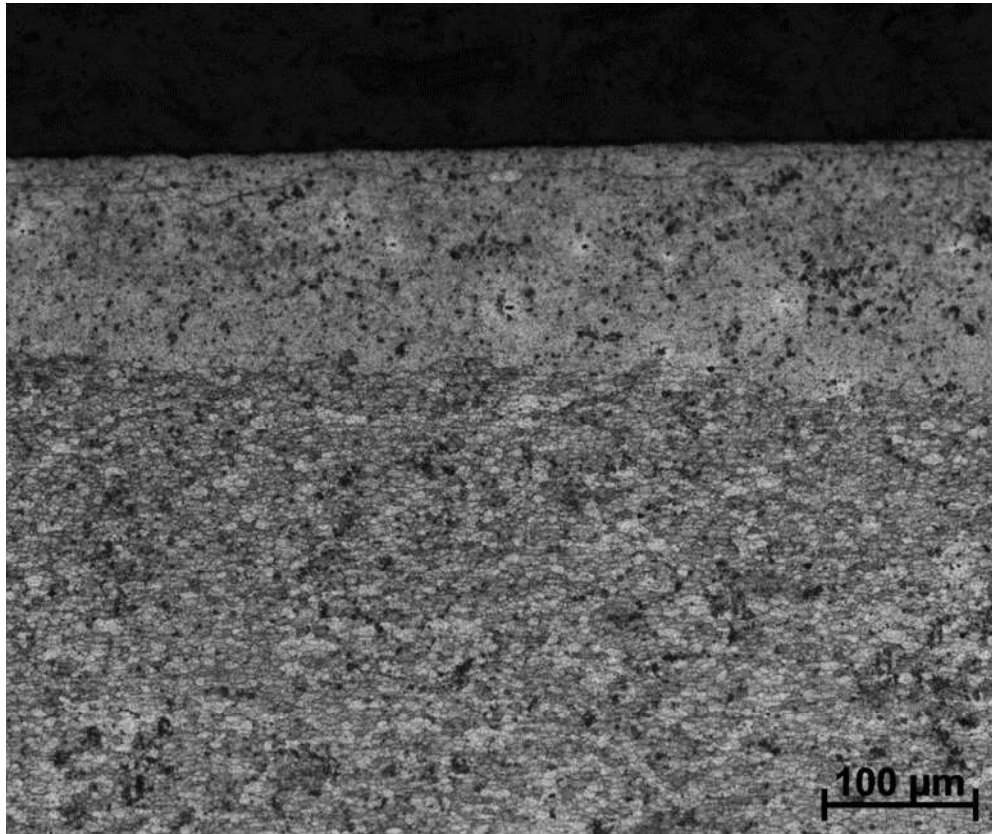


Figure 24 – Surface of the sample 12X(EXT)

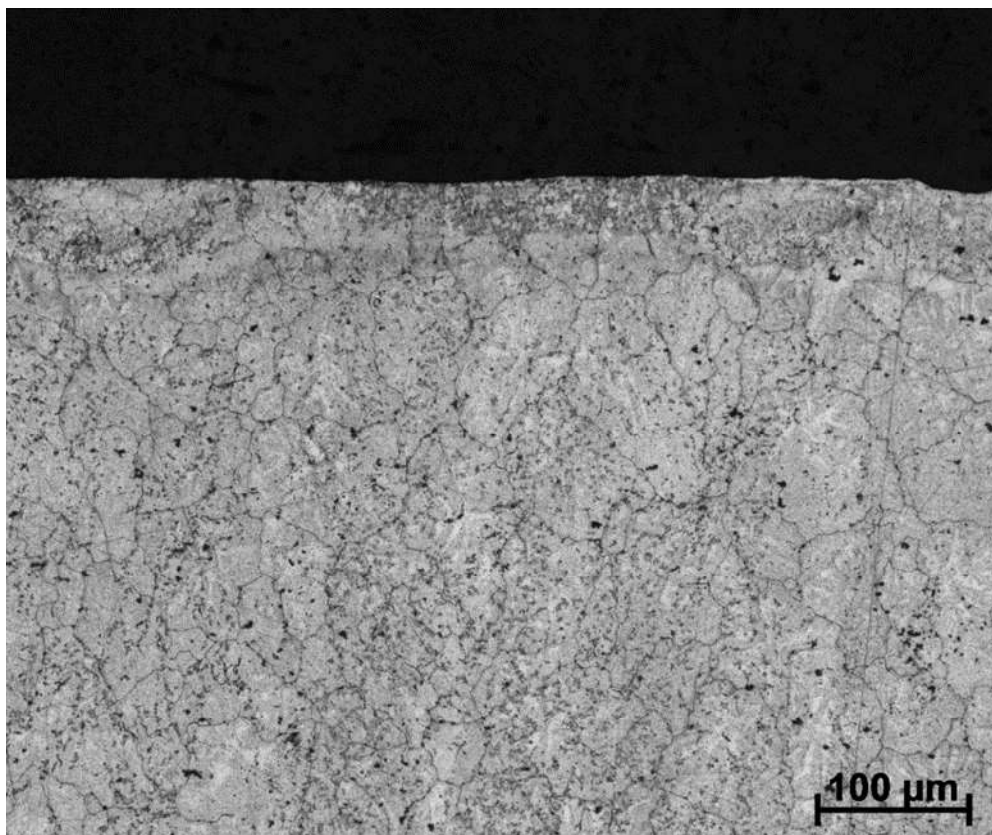


Figure 25 - Surface of the sample 22X(HCM)

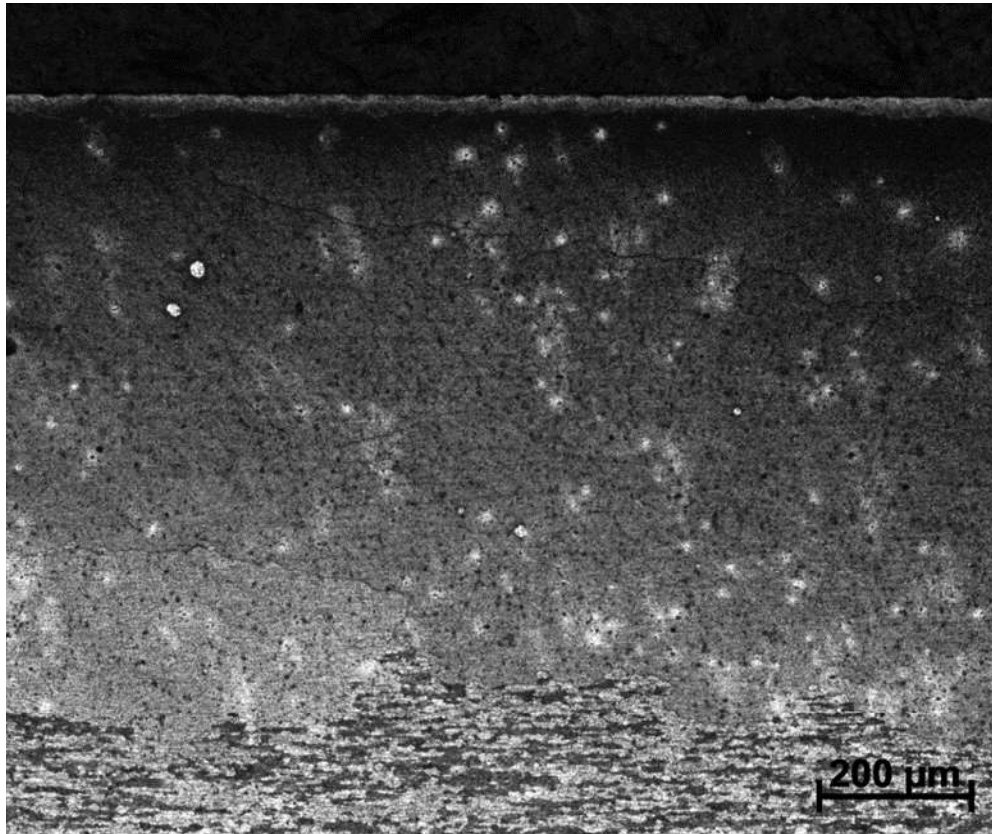


Figure 26 - Surface of the sample 14X(EXT)

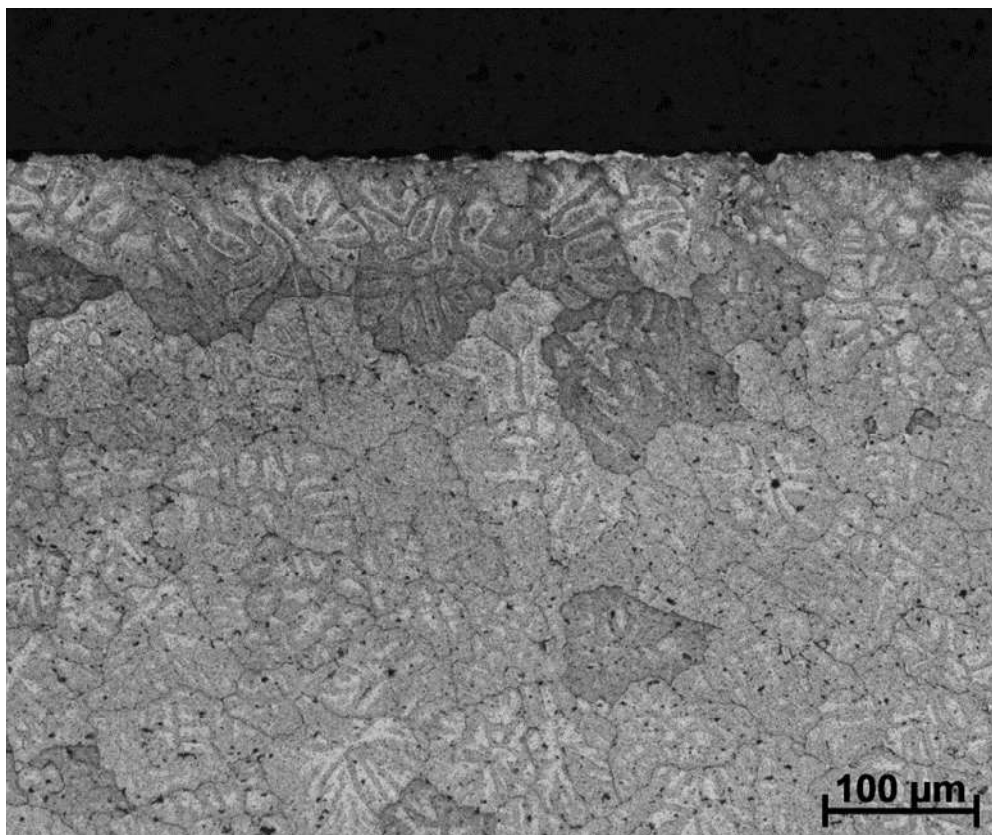


Figure 27 - Surface of the sample 24X(HCM)

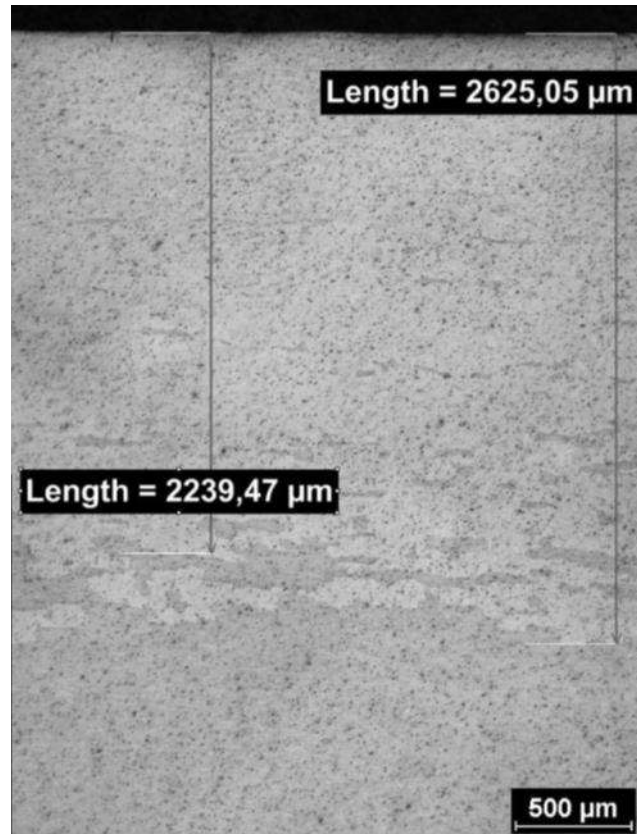


Figure 28 - Surface of the sample 17X(EXT)

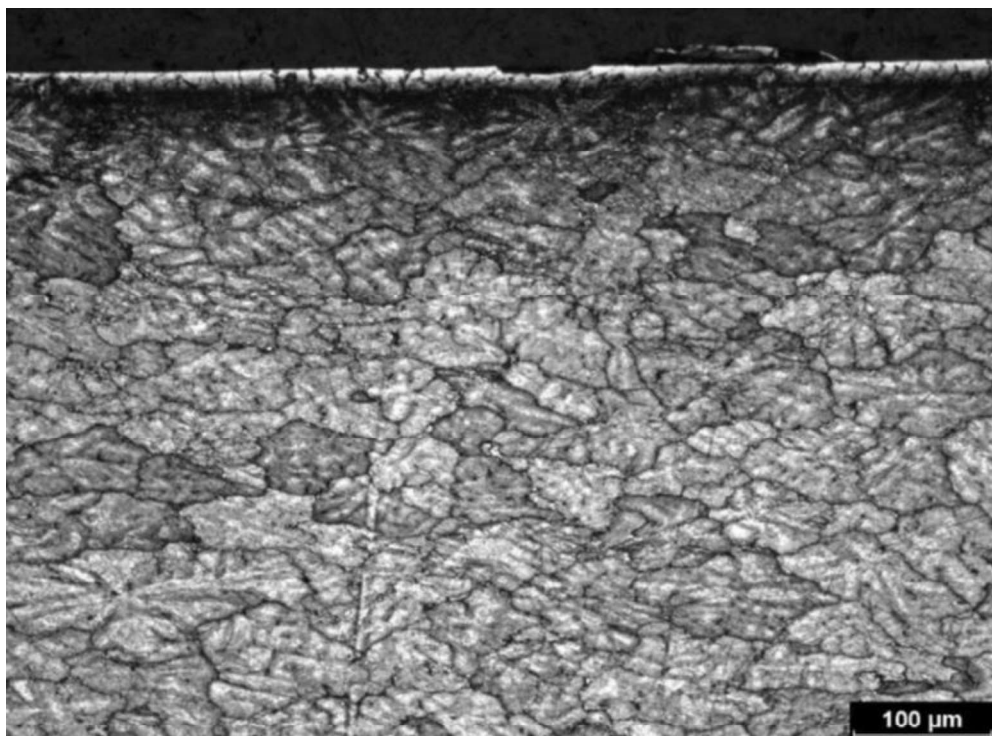


Figure 29 - Surface of the sample 27X(HCM)

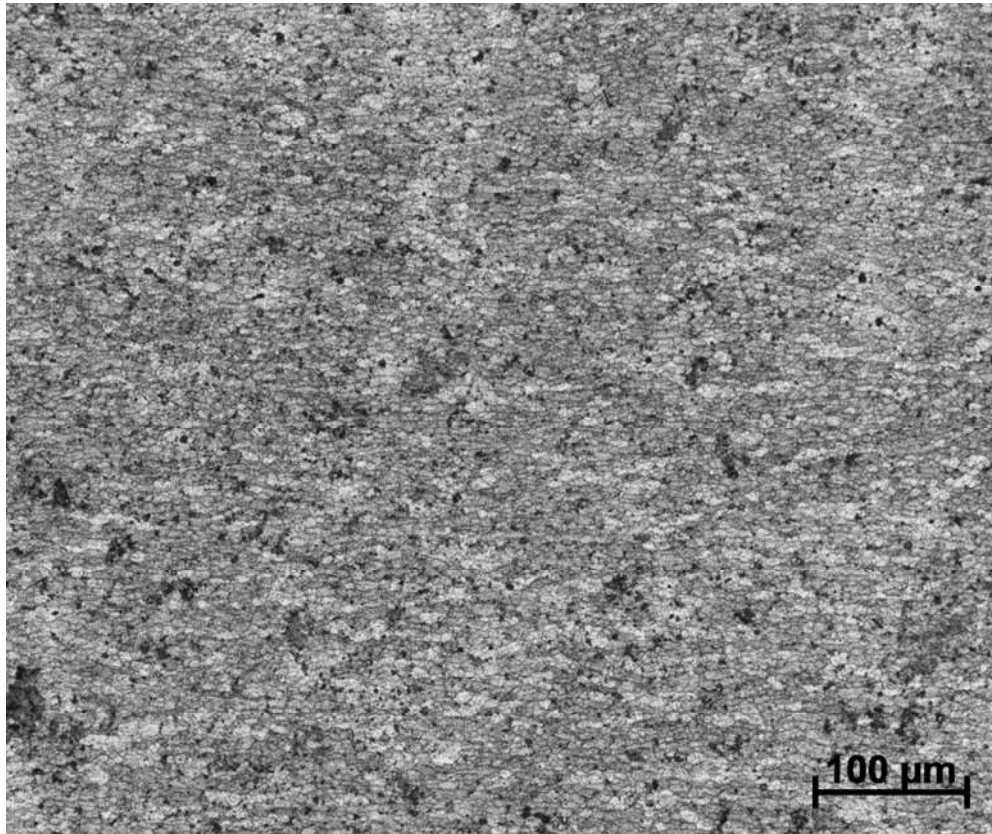


Figure 30 - Core of the sample 12X(EXT)

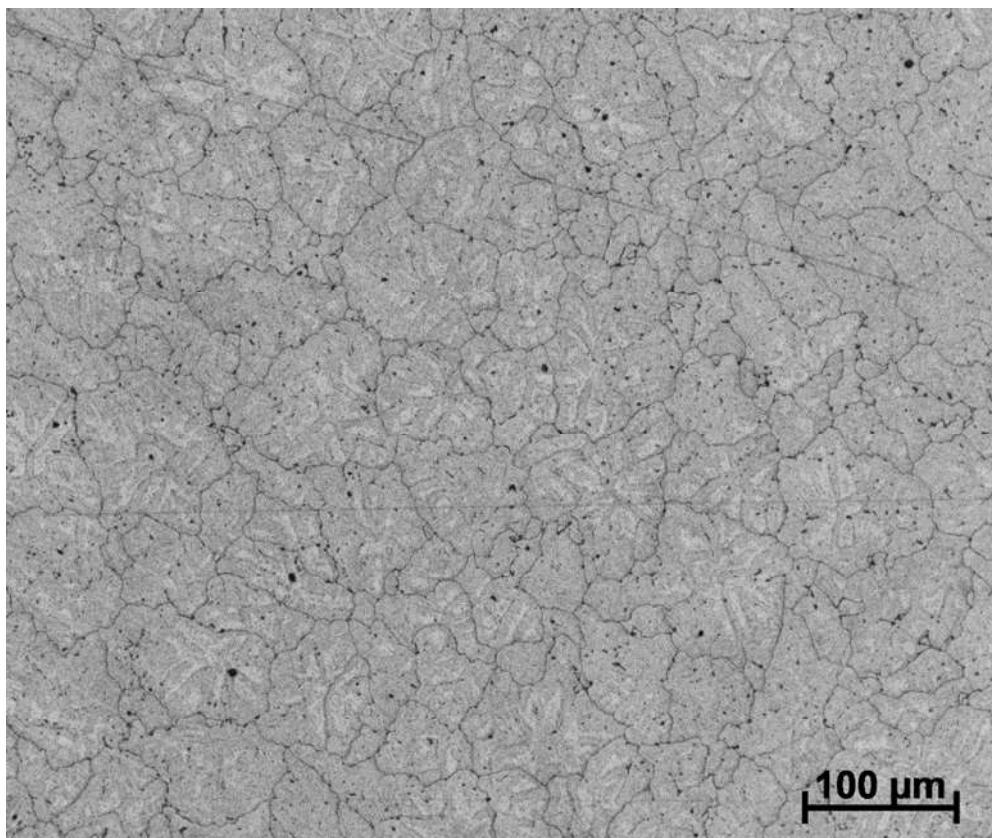


Figure 31 - Core of the sample 22X(HCM)

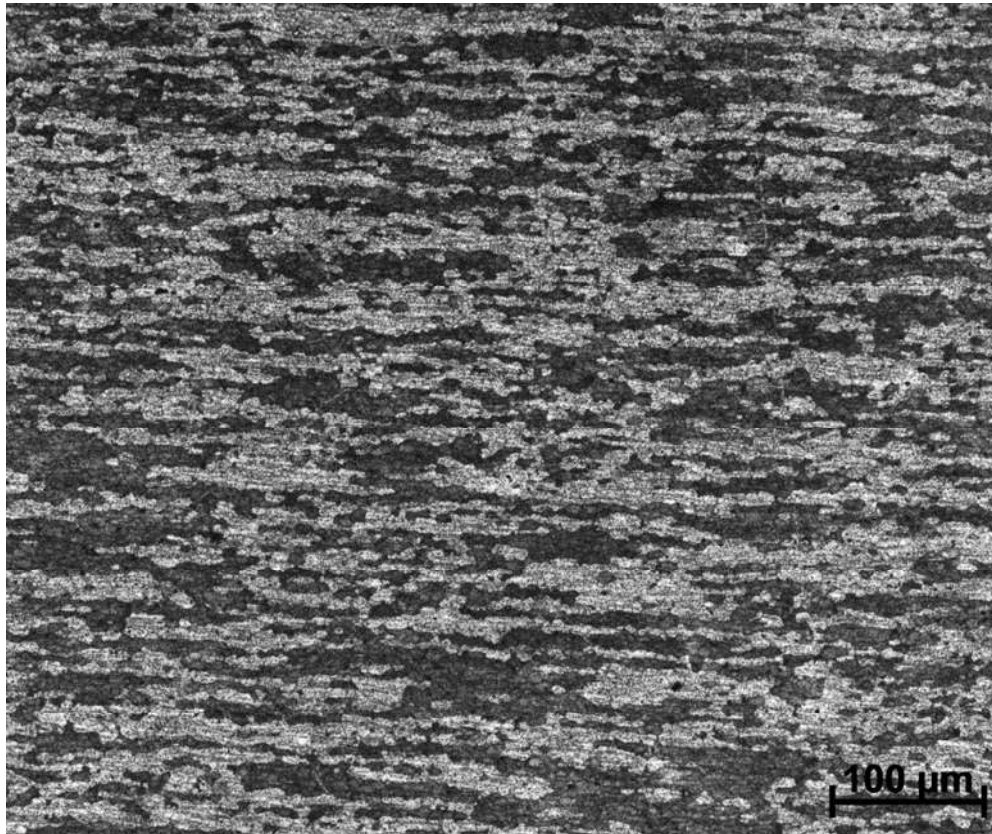


Figure 32 - Core of the sample 14X(EXT)

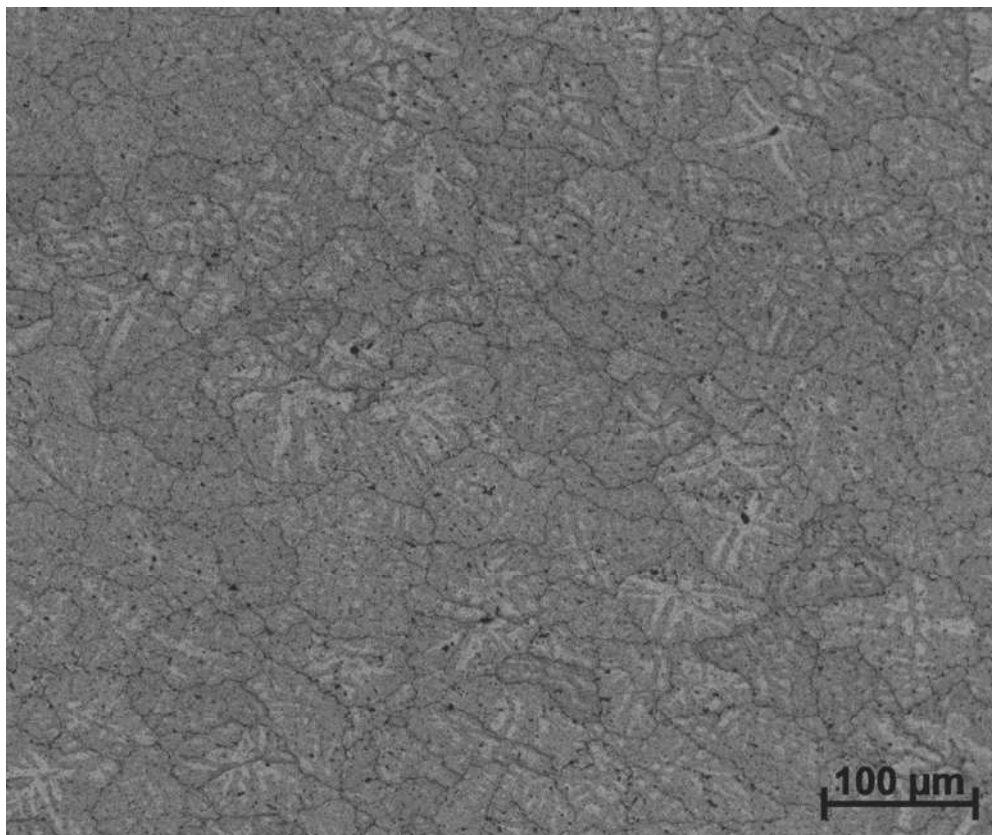


Figure 33 - Core of the sample 24X(HCM)

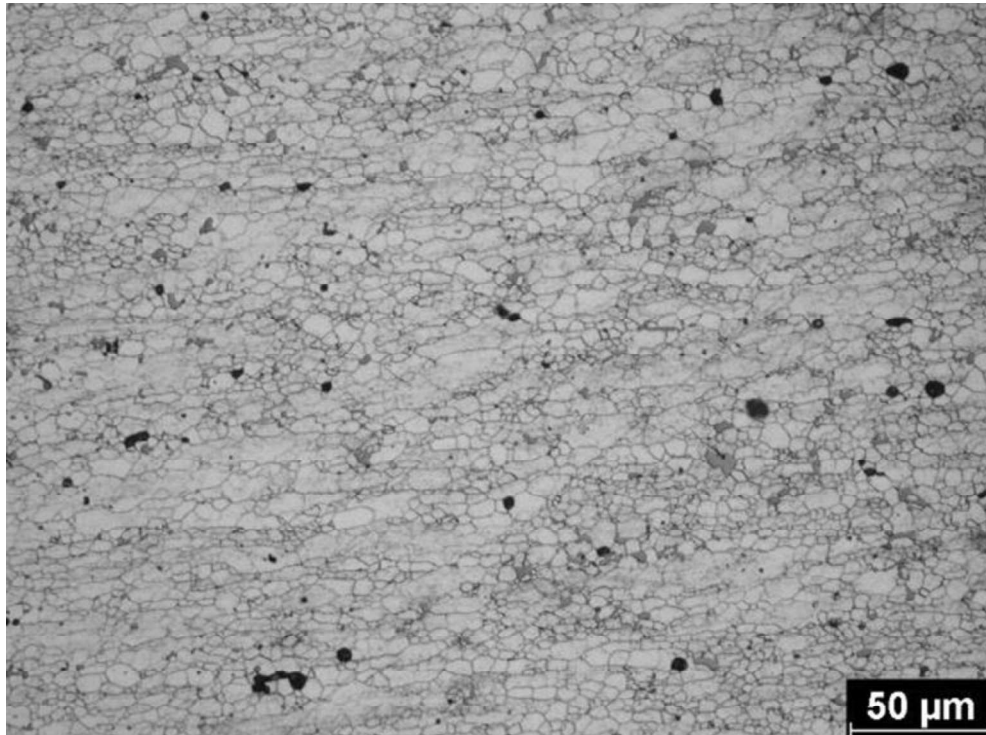


Figure 34 - Core of the sample 17X(EXT)



Figure 35 - Core of the sample 27X(HCM)

The microstructures of the samples show the following trends:

By default, the two semi-finished products differ in their structure. The extruded one has a deforming fibrous structure with grain elongation in the pressing direction. In contrast, the semi-finished product produced by the HCM method has a dendritic structure with undeformed grains.

The extruded one has been found to have a coarse-grained surface layer in the longitudinal direction of 500 μm to several millimeters. It has been found in the HCM semi-finished product that, even after deformation and deformation with heat treatment, the grain does not coarse in the surface layer and does not significantly change its shape.

In the core area, a significantly finer structure was observed in the extruded semi-finished products irrespective the deformation and heat treatment than in the HCM semi-finished products. Due to the light microscopy limits to determine whether it is a grain boundary or only a sub-grain boundary, the EBSD analysis was proceeded.

A more detailed evaluation of the structural parameters, such as grain size or size of the surface recrystallized layer, is contained in the final works of my colleagues.

12.2 Electron backscatter diffraction

EBS D utilizes BSE diffraction on a crystal lattice. This method allows to study UFG materials produced by SPD methods. It is possible to determine the crystallographic grain orientation, grain size and grain orientation. After the interaction with the crystalline material, the electron scatters, the diffraction occurs on the crystal planes in the directions given by Bragg's law

$$n\lambda = 2d \sin \theta$$

where n is the order of reflection, λ is the wavelength, d is the interplanar distance of the diffracting warp of the crystallographic planes, and θ is the angle of incidence and reflection of the electrons, the so-called Bragg angle. The diffraction pattern is then captured by means of a phosphor screen on which Kossel circles are projected.

This method is very sensitive to surface quality, so ion polishing is highly recommended for sample preparation. [18]

The HKL system was used to analyze the relative angles of misorientation of adjacent grains. EBSD maps were collected at SEM JEOL JSM-7600F an accelerating voltage of 30 kV, the size of the scanned fields and the size of the steps were varied due to the grain size.

Grain boundaries with misorientation between 2° and 10° were considered LAGB Low-angle and boundaries with misorientation higher than 10° were HAGB. Grain boundaries with a misorientation lower than 2° were excluded from the evaluation because of high orientation noise for highly deformed materials. This noise in orientation maps is due to tracks that are indexed incorrectly. This noise can be filtered out, especially for annealed and slightly deformed materials.

Using the EBSD, it was compared which semi-finished products has a greater tendency to form recrystallized grains and which has a greater tendency to regulate the grain orientation of the structure.

Fig. 36 and 37 show to what extent the core structure of both semi-finished products was recrystallized after 20% deformation and heat treatment. The red lines are the grain boundaries, the green lines are sub-grains boundaries.

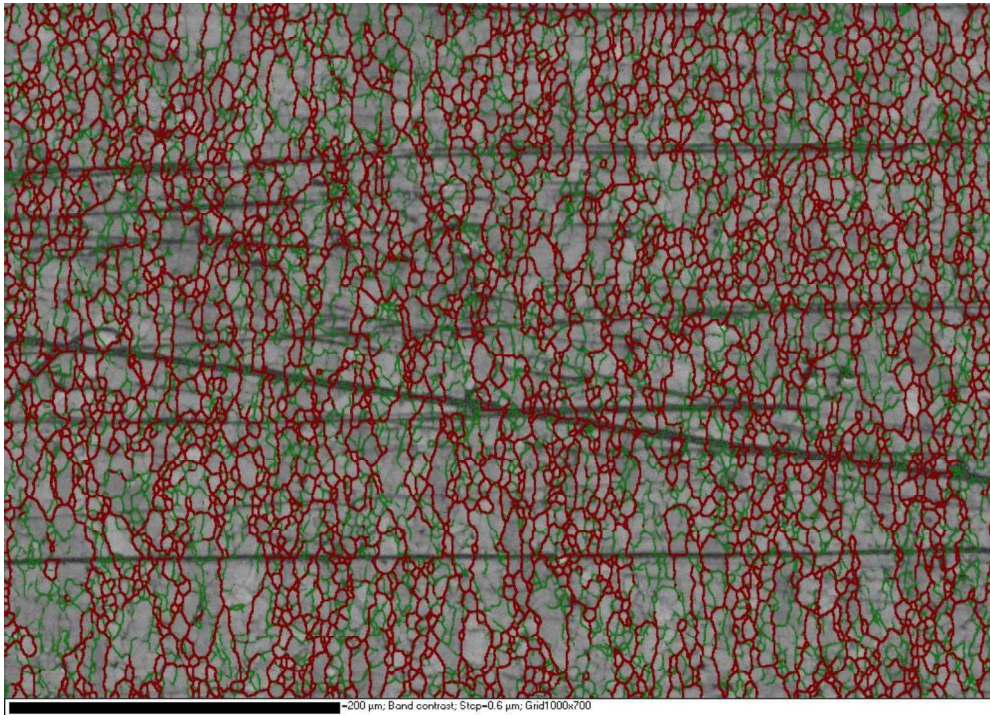


Figure 36 – HAGB and LAGB in the sample 12X(EXT)

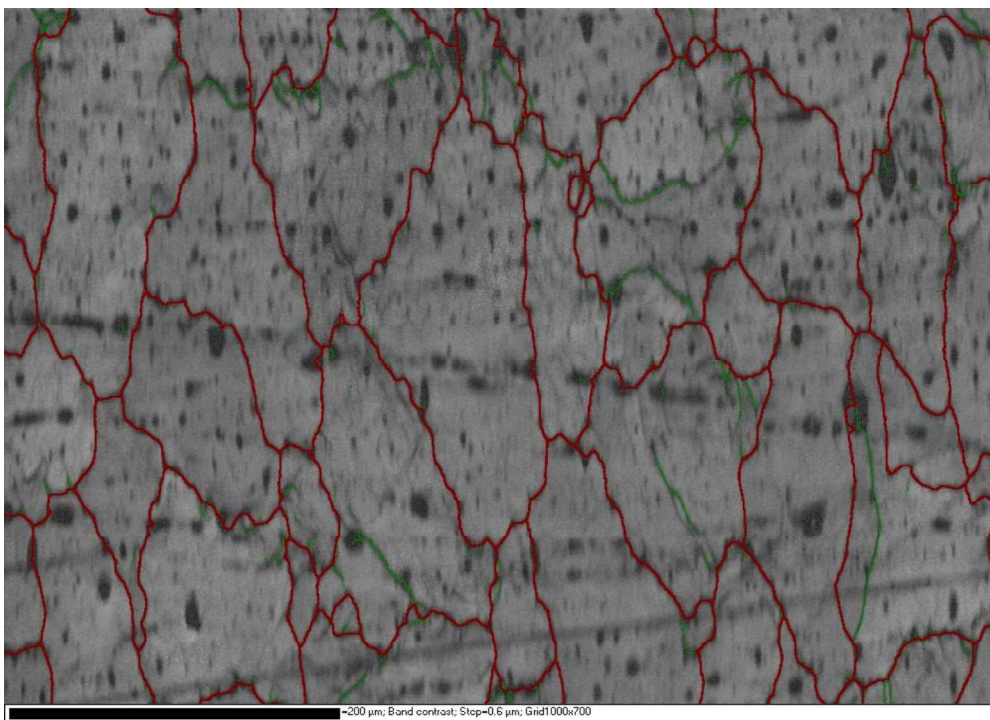


Figure 37 - HAGB and LAGB in the sample 22X(HCM)

It can be seen from Fig. 36 and 37 that the extruded semi-finished products exhibits a significantly greater number of low-angle grain boundaries and thus recrystallized grains than the HCM semi-finished products.

Fig. 38 and 39 show to what extent the core structure of both samples was recrystallized after 40% deformation and heat treatment.

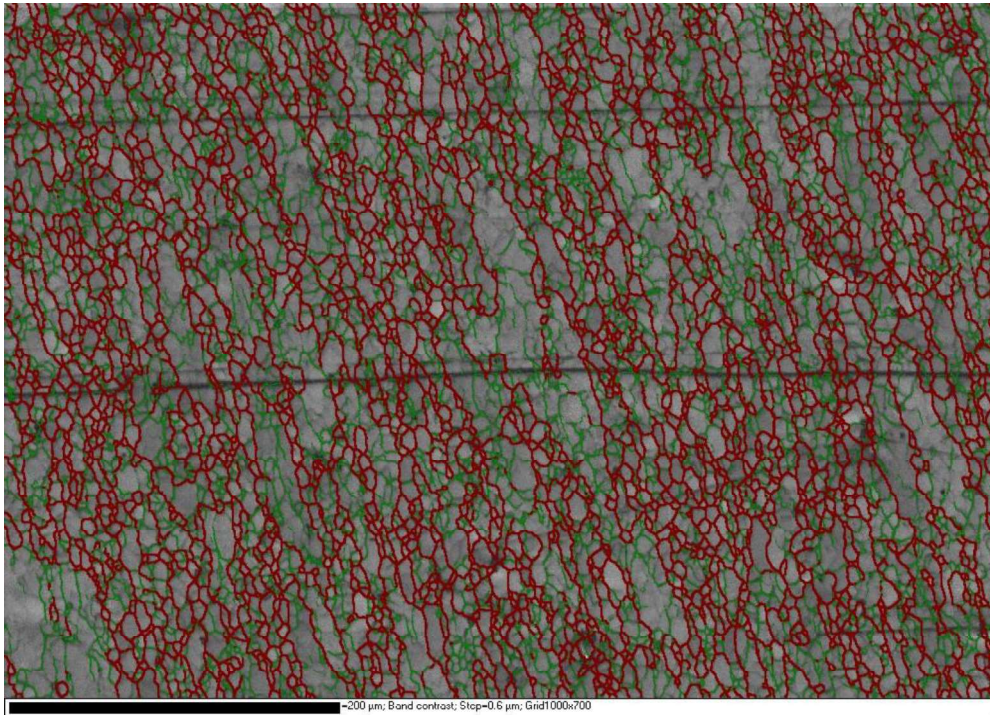


Figure 38 - HAGB and LAGB in the sample 14X(EXT)

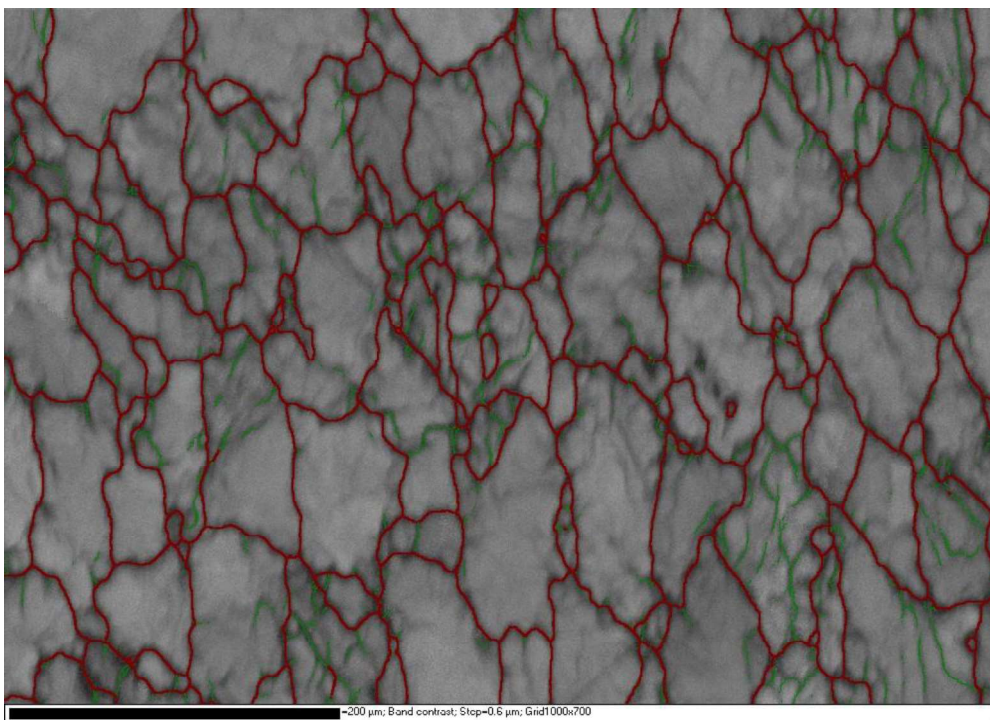


Figure 39 - HAGB and LAGB in the sample 24X(HCM)

It can be seen from Fig. 38 and 39 that the extruded semi-finished products exhibits a significantly greater number of low-angle grain boundaries and thus recrystallized grains than the HCM semi-finished products.

Fig. 40 and 41 show how the core structure, of both semi-finished products after 20% deformation and heat treatment, is oriented.

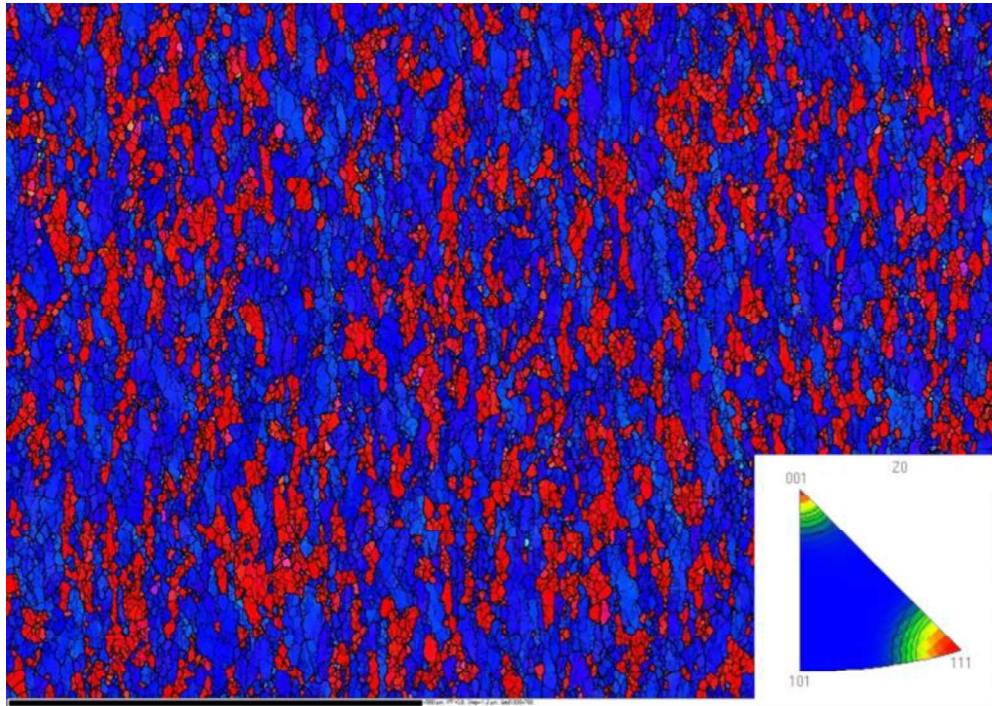


Figure 40 - The orientation of the grains in the sample 12X(EXT)

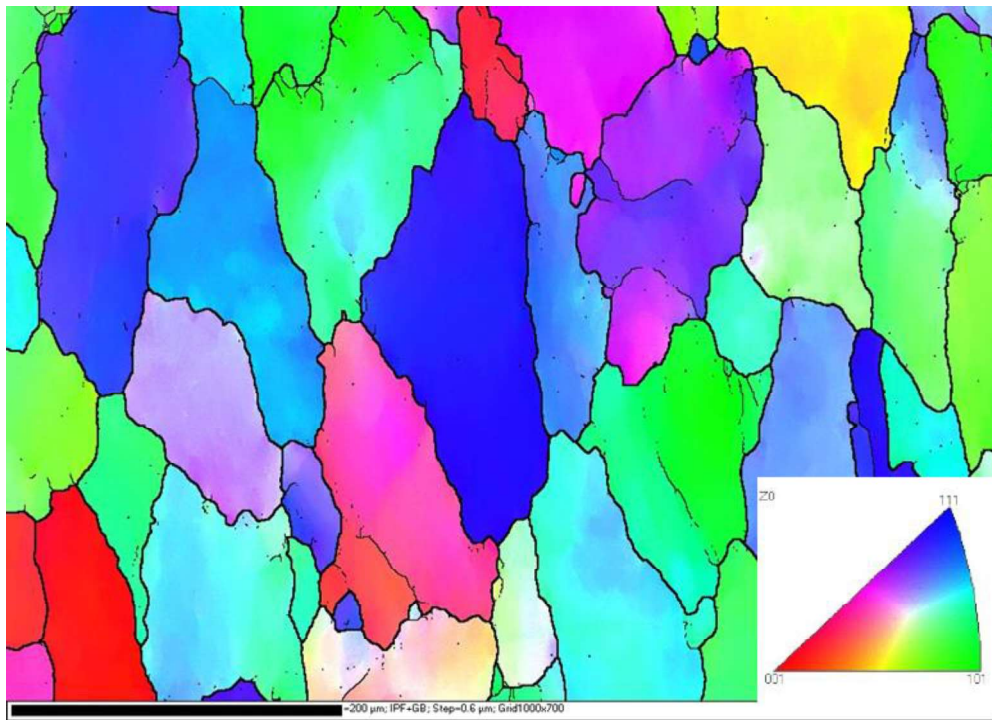


Figure 41 - The orientation of the grains in the sample 22X(HCM)

It can be seen from Fig. 40 and 41 that the extruded semi-finished product has a orientated structure from which it is possible to determine the direction of forming. In contrast, the HCM semi-finished products exhibits by chance a grain orientation that is not deformed.

Fig. 42 and 43 show how the core structure of both semi-finished products is oriented after 40% deformation and heat treatment.

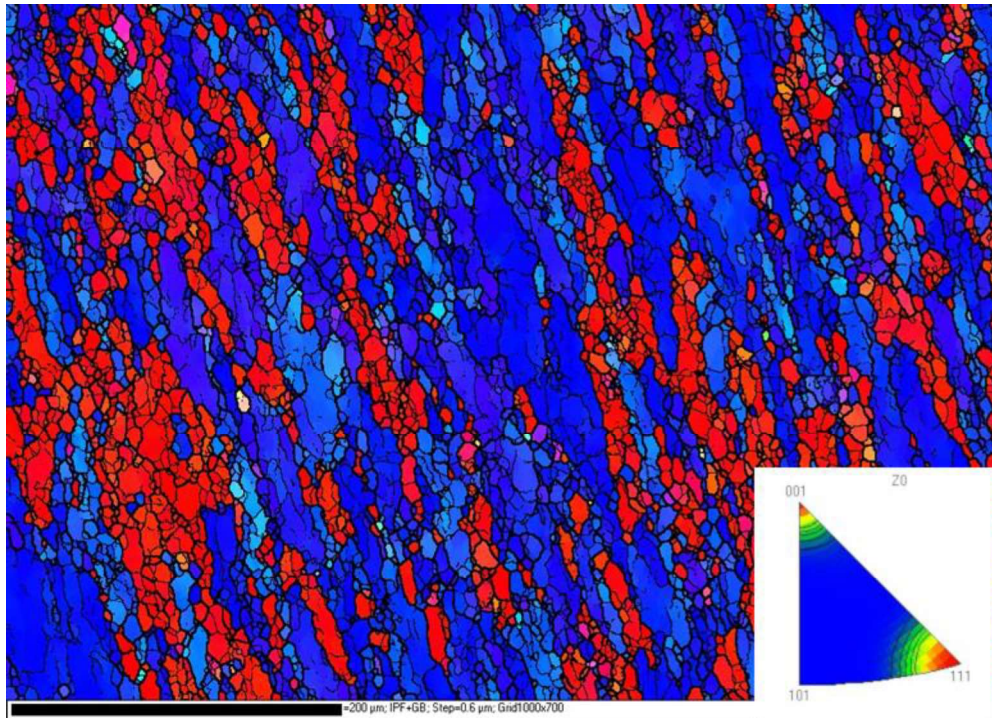


Figure 42 – The orientation of the grains in the sample 14X(EXT)

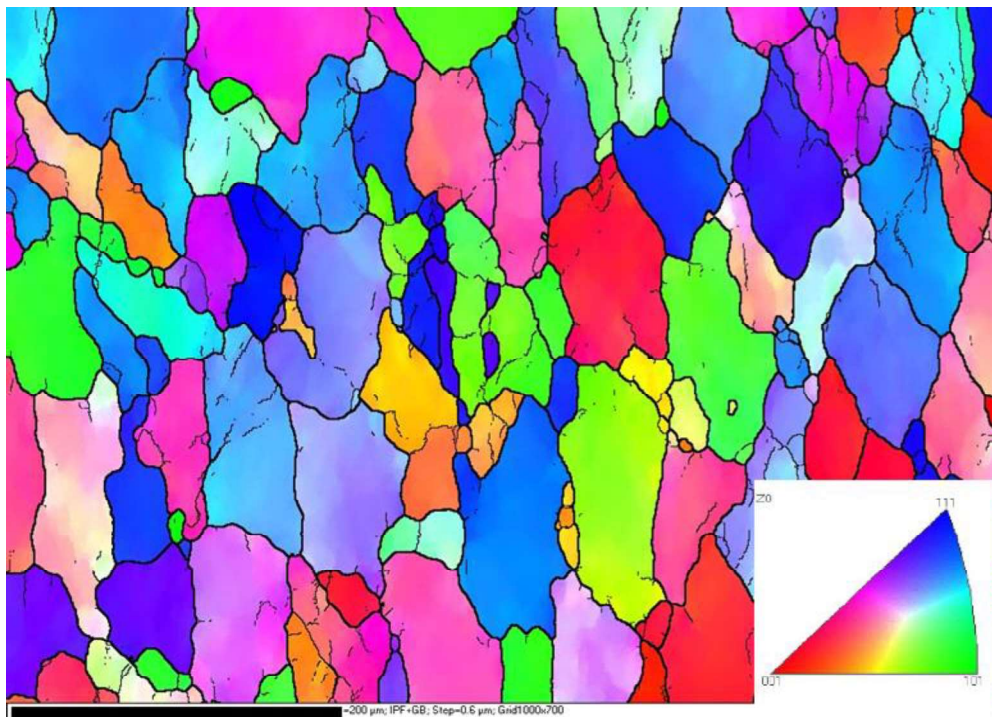


Figure 43 - The orientation of the grains in the sample 24X(HCM)

It can be seen from Fig. 42 and 43 that the extruded semi-finished product has a orientated structure from which it is possible to determine the direction of forming. On the other hand, the HCM semi-finished product has a random grain orientation, but there is already a grain orientation occurring during the deformation. The results of the EBSD show, that the grain size of extruded semi-finished products cannot be unambiguously determined by light microscopy due to the impossibility of distinguishing grain boundaries from sub grain boundaries, the number of which increases with both deformation and heat treatment.

13 The hardness of the samples

Hardness is defined as the resistance of a material to an indentation of the foreign object. There are several methods that differ in the manner of measuring or geometry of the indenter. One option is the Vickers measurement method. In this method, the indenter has the shape of a quadrilateral pyramid with an apex angle of 136° . The indenter is pressed into the material by the load F , the load time is 10 to 15 seconds. For the evaluation of the test, the lengths of the two diagonals of the indentation formed are measured and their arithmetic diameter d is calculated. The resulting hardness value is dimensionless and calculated from

$$HV = 0,1891 \frac{F}{d^2}$$

where F is a force and d is an arithmetic mean of the diagonals.

The hardness measurement was performed according to the Vickers method according to the valid standard ČSN EN ISO 6507-1. The measurement was performed on a Zwick hardness tester with load HV 1, nominal load 9.807 N. The resulting value is the arithmetic mean of these values. Metallographic samples were measured in the core and surface area. [19]

13.1 Extruded semi-finished products

Tab. 12, 13 and 14 shown results of the hardness tests of extruded semi-finished products. The results are compared in Fig. 44 and 45.

Table 12 - The hardness of the extruded samples in transection

Sample	Location	HV1	ØHV1	Sample	Location	HV1	ØHV1
1PO	Core	92	91	1POX	Core	115	116
		90				116	
	Surface	93	93		Surface	110	111
		93				111	
12PO	Core	43	42	12POX	Core	97	97
		41				97	
	Surface	42	42		Surface	95	94
		41				93	
14PO	Core	39	40	14POX	Core	96	95
		41				93	
	Surface	39	39		Surface	95	94
		38				93	
124PO	Core	45	44	124POX	Core	112	109
		43				105	
	Surface	50	51		Surface	102	103
		52				103	
142PO	Core	42	43	142POX	Core	112	113
		44				113	
	Surface	48	48		Surface	109	109
		48				108	
17PO	Core	45	45	17POX	Core	112	113
		45				113	
	Surface	43	46		Surface	106	106
		48				106	

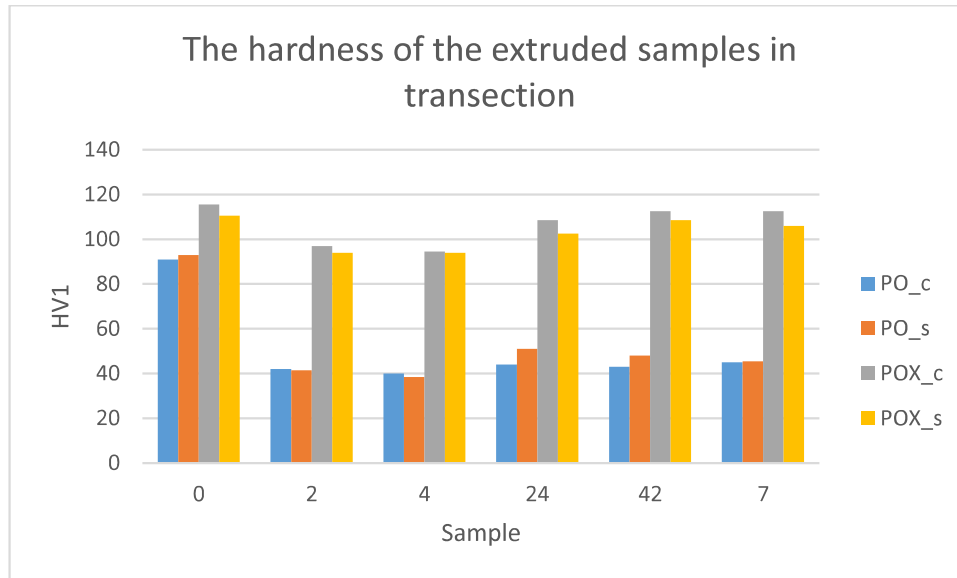


Figure 44 - The hardness values for extruded samples in transection

Table 13 - The hardness of the extruded samples in cross section

Sample	Location	HV1	ØHV1	Sample	Location	HV1	ØHV1
1PR	Core	88	91	1PRX	Core	110	109
		93				107	
	Surface	83	83		Surface	108	105
		83				101	
12PR	Core	40	41	12PRX	Core	95	97
		42				99	
	Surface	38	38		Surface	97	96
		38				95	
14PR	Core	41	41	14PRX	Core	98	99
		40				99	
	Surface	40	39		Surface	94	96
		38				97	
124PR	Core	49	47	124PRX	Core	112	112
		45				111	
	Surface	42	43		Surface	100	105
		43				109	
142PR	Core	49	49	142PRX	Core	106	105
		48				103	
	Surface	47	47		Surface	104	101
		46				97	
17PR	Core	42	42	17PRX	Core	111	115
		42				119	
	Surface	44	46		Surface	101	109
		48				106	

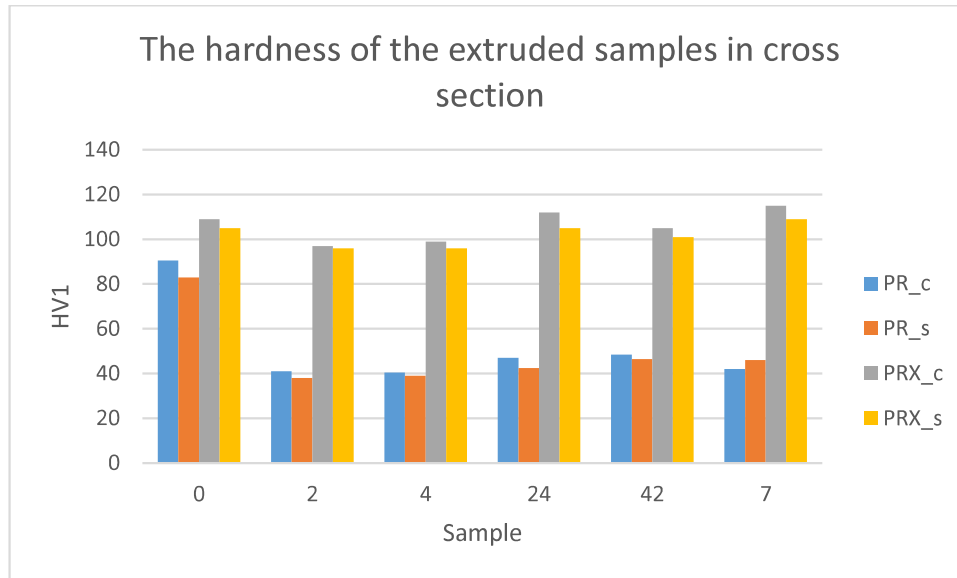


Figure 45 - The hardness values for extruded samples in cross section

Table 14 – Increase of hardness in extruded samples

Sample	$\Delta HV1$
0	21
2	55
4	56
24	61
42	60
7	66

The following trends are evident from the hardness tests of extruded samples.

The resulting hardness values do not differ significantly depending on the sampling direction.

The supplied extruded semi-finished products that have not been heat treated show increased hardness values of approximately 50 Vickers compared to non-thermally processed samples with little deformation.

The surface of the sample usually shows lower hardness within the units of Vickers than the core.

Heat treatment of the non-deformed extruded semi-finished products can increase its hardness by approximately 20 Vickers.

The hardness of the deformed extruded samples increased by approximately 55 to 65 Vickers with heat treatment. The highest increase in hardness values was measured for sample 7.

13.2 HCM semi-finished products

Tab. 15, 16 and 17 shown results of the hardness tests of HCM semi-finished products. The results are compared in Fig. 46 and 47.

Table 15 - The hardness of the HCM semi-finished products in transection

Sample	Location	HV1	ØHV1	Sample	Location	HV1	ØHV1
2PO	Core	70	72	2POX	Core	107	107
		73				106	
	Surface	62	61		Surface	106	107
		59				108	
22PO	Core	44	45	22POX	Core	93	94
		46				94	
	Surface	44	43		Surface	91	95
		42				99	
24PO	Core	43	43	24POX	Core	97	98
		42				99	
	Surface	42	43		Surface	96	98
		43				100	
224PO	Core	49	49	224POX	Core	110	112
		49				114	
	Surface	47	47		Surface	106	108
		46				109	
242PO	Core	51	51	242POX	Core	114	115
		50				115	
	Surface	45	47		Surface	108	111
		48				113	
27PO	Core	51	53	27POX	Core	114	116
		55				118	
	Surface	54	54		Surface	109	111
		48				106	

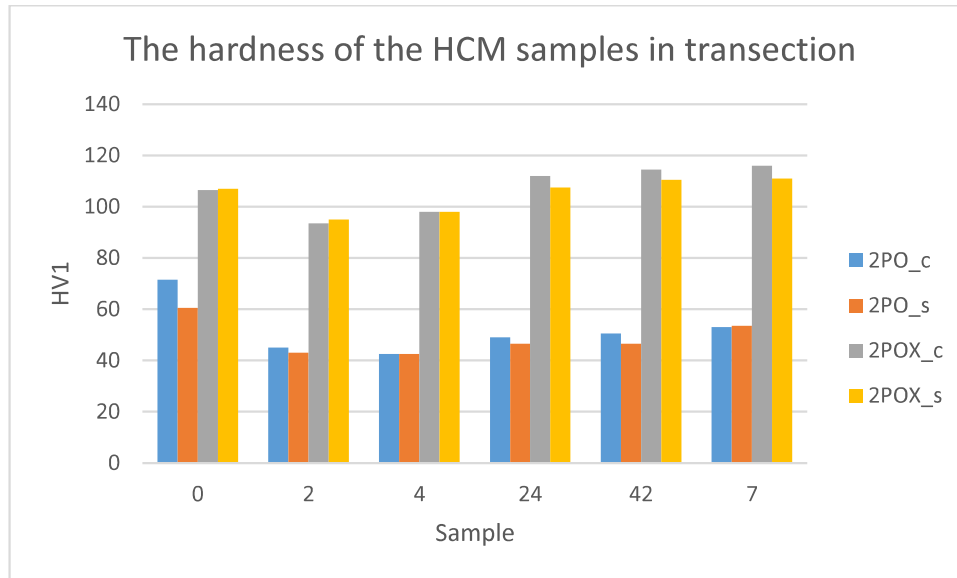


Figure 46 - The hardness values for HCM samples in transection

Table 16 - The hardness of the HCM semi-finished products in cross section

Sample	Location	HV1	ØHV1	Sample	Location	HV1	ØHV1
2PR	Core	73	75	2PRX	Core	114	114
		77				114	
	Surface	60	61		Surface	106	107
		61				107	
22PR	Core	41	42	22PRX	Core	96	95
		42				95	
	Surface	42	43		Surface	95	94
		43				93	
24PR	Core	43	43	24PRX	Core	101	99
		43				98	
	Surface	42	43		Surface	95	97
		43				98	
224PR	Core	50	51	224PRX	Core	110	111
		51				112	
	Surface	48	49		Surface	106	108
		50				109	
242PR	Core	50	51	242PRX	Core	113	115
		52				116	
	Surface	46	47		Surface	103	105
		48				106	
27PR	Core	54	56	27PRX	Core	118	115
		57				112	
	Surface	51	53		Surface	111	111
		48				106	

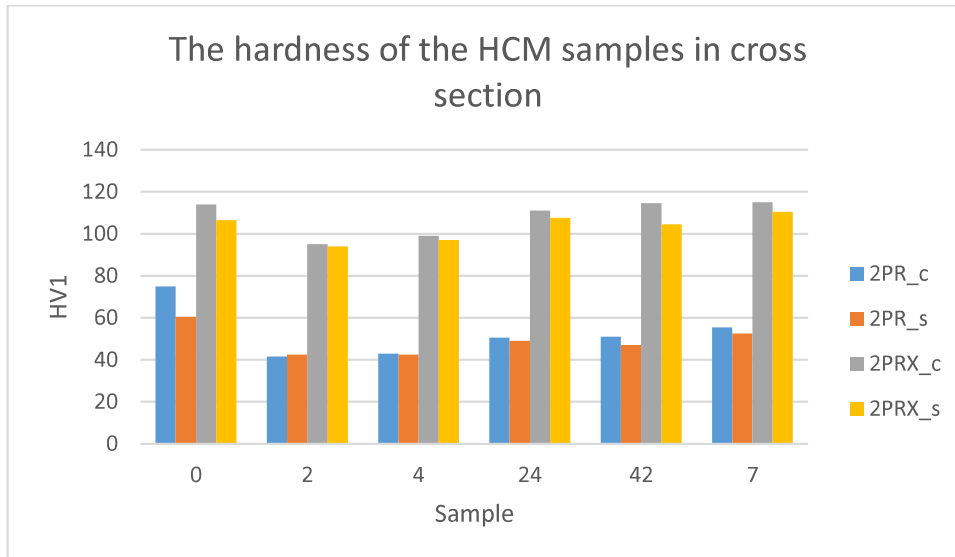


Figure 47 - The hardness values for HCM samples in cross section

Table 17 - Increase of hardness in HCM samples

Sample	$\Delta HV1$
0	42
2	51
4	55
24	61
42	62
7	60

The following trends are evident from the hardness tests of HCM samples.

The resulting hardness values do not differ significantly depending on the sampling direction.

The supplied HCM semi-finished products that have not been heat treated show increased hardness values of approximately 30 Vickers compared to non-thermally processed samples with little deformation.

The surface of the sample usually shows lower hardness within the units of Vickers than the core.

Heat treatment of the non-deformed HCM semi-finished products can increase its hardness by approximately 40 Vickers.

The hardness of the deformed HCM samples increased by approximately 50 to 60 Vickers with heat treatment. The highest increase in hardness values was measured for samples 24, 42 and 7.

13.3 Comparison of the hardness test results

It can be seen from Fig. 48 that, of the unheat-treated samples, the highest hardness values are those produced from the supplied semi-finished products. By heating to the forging temperature and subsequent deformation, these values are significantly reduced. Then the hardness values show an upward trend along with the degree of deformation.

It can be observed from Fig. 49 that the heat-treated samples have a slightly harder core than the surface and the hardness value increases with the degree of deformation. There is no significant difference between HCM and extruded semi-finished products.

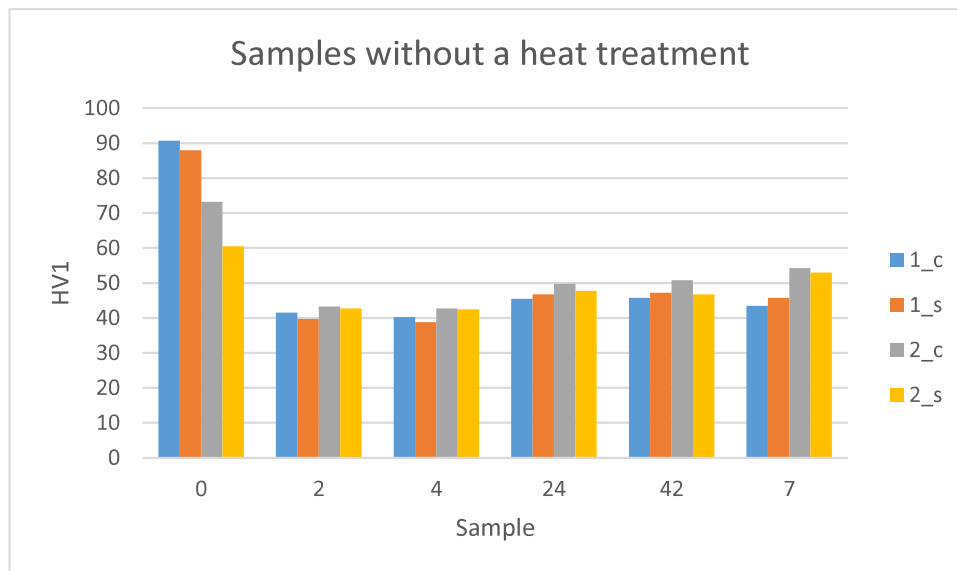


Figure 48- The hardness values for all the samples without a heat treatment

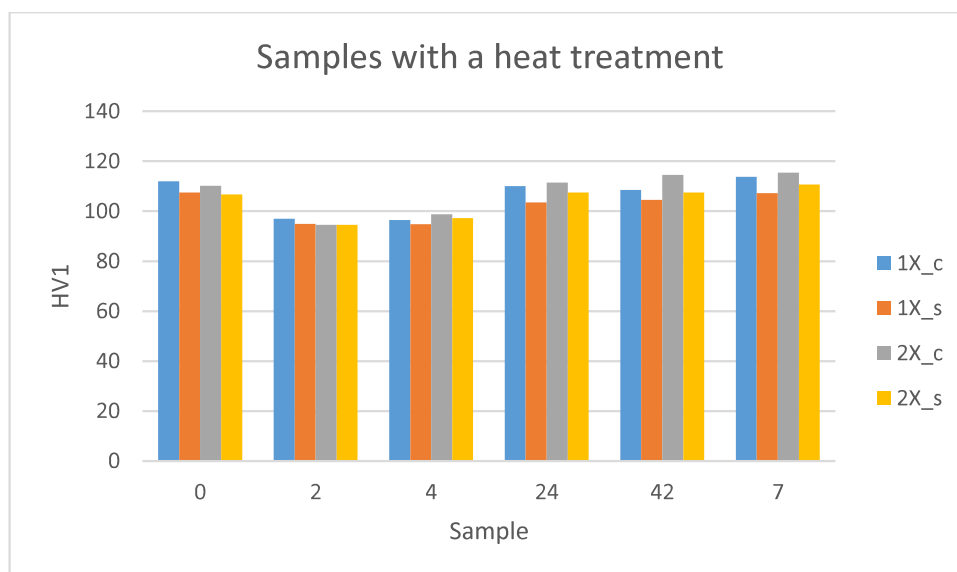


Figure 49 - The hardness values for all the samples with a heat treatment

Table 18 - Increase of hardness in both semi-finished products

Sample	$\Delta HV1$ in EXT	$\Delta HV1$ in HCM
0	21	42
2	55	51
4	56	55
24	61	61
42	60	62
7	66	60

It can be observed from Tab. 18 that the largest difference in hardness increase occurred in the undeformed sample. No significant differences were observed in the deformed samples.

Fig. 50 shows the hardness values for the 12PRX sample. The hardness was measured at different loads to verify that the inaccuracy typical of very low loads was already eliminated for load 1 kgf.

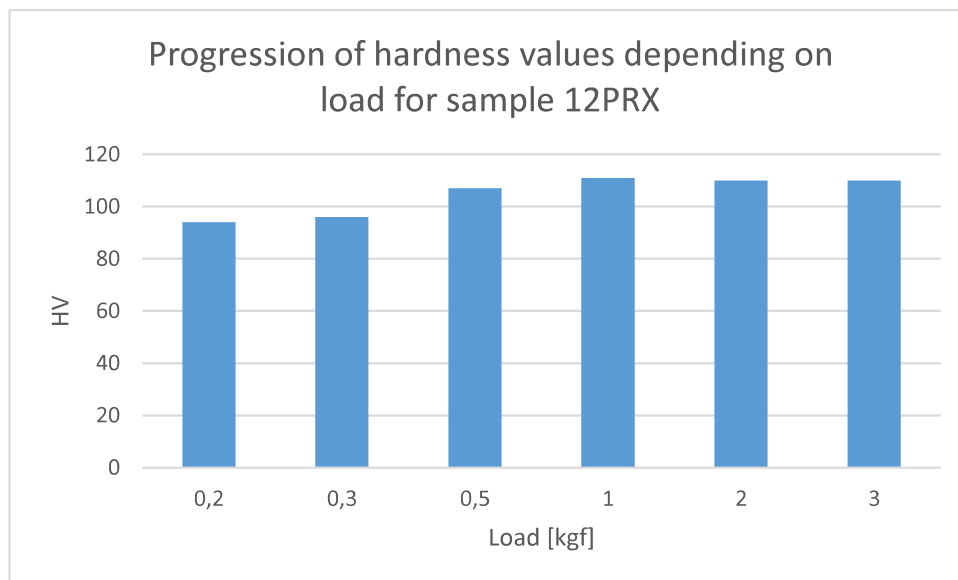


Figure 50 - Progression of hardness values depending on load for sample 12PRX

Conclusion

The effect of deformation on recrystallization of aluminum alloy EN AW 6082 was studied on two differently manufactured semi-finished products – extruded and HCM.

The macrostructure evaluation revealed that the specimens prepared from the extruded semi-finished products produce a visible coarse-grained surface layer after deformation, which increases with heat treatment, with a layer thickness of up to 6 mm. This phenomenon was not observed in samples from the HCM semi-finished products.

Mechanical properties ($R_{p0.2}$, R_m , A , Z) were evaluated by tensile test. From the tensile test results, it was found that the supplied HCM samples had lower strength properties than extruded. By deformation and subsequent heat treatment, the strength properties are almost equal to the extruded semi-finished product. Slightly higher ductility values were found in the HCM sample in accordance with a more homogeneous microstructure.

Significant differences in the structure of the semi-finished products were observed by microstructure evaluation using light microscopy. While the supplied extruded semi-finished products have a deformation fiber structure with grain orientation in the extruding direction, the HCM semi-finished products have a dendritic structure with equiaxed grains.

It has been observed with the extruded samples that the grains in the coarse-grained surface layer are elongated. The width of the coarse-grained layer of heat-treated samples increased with increasing degree of deformation. The size of these grains in the longitudinal direction ranged from 500 μm to several mm. It has been found in the HCM semi-finished product that, even after deformation and deformation with heat treatment, the grain does not coarsen in the surface layer and does not significantly change its shape.

On the extruded samples, a fine grain structure was observed in the core, even at small deformations. The HCM samples, at the same degree of deformation, showed a coarser structure. The core structure of these two semi-finished products was aligned after a high degree of deformation (70%) and subsequent heat treatment.

One of the limits of light microscopy is the inability to distinguish between grain boundaries and sub-grains furthermore, the grain orientations cannot be determined. Electron backscatter diffraction is used to evaluate these parameters.

It is evident from the EBSD that the extruded samples have a strongly oriented structure from the production. The structure of HCM samples begins to become oriented with increasing degree of deformation. Even from small deformations, a large number of sub-grain boundaries can be observed on extruded specimens and thus a much more recrystallizable structure than HCM specimens of the same deformation.

The results of the hardness measurements show no significant differences in hardness depending on the sampling direction. The core hardness is usually slightly higher than the surface hardness. A marked increase in hardness is evident in all cases of samples after heat treatment. There are no significant differences in hardness values between HCM and extruded samples.

Comparison of the results of structure evaluation and mechanical properties shows that the HCM semi-finished product, after deformation and heat treatment, are at least as good as the extruded semi-finished product. The HCM semi-finished products have slightly better ductility. And a significant advantage of the HCM semi-finished products is resistance to grain coarsening in the surface layer.

BIBLIOGRAPHY

- [1] *Encyklopedie hliníku*. Děčín: Alcan Děčín Extrusions, 2005. ISBN 8089041884.
- [2] CALLISTER, William. *Materials science and engineering: an introduction*. 7th ed. New York: John Wiley, 2007. ISBN 978-0-471-73696-7.
- [3] KŘÍŽ, Rudolf a Pavel VÁVRA. *Strojírenská příručka: 24 oddílů v osmi svazcích*. Praha: Scientia, 1993. ISBN 80-858-2723-9.
- [4] *Asm Handbook: Properties and Selection : Nonferrous Alloys and Special-Purpose Materials (Asm Handbook) VOL. 2*. b.r.
- [5] *Aluminum and aluminum alloys*. Materials Park, OH: ASM International, 1993. ISBN 978-087-1704-962.
- [6] *Hliník a slitiny hliníku - Chemické složení a druhy tvářených výrobků*. Praha: Český normalizační institut, 2003.
- [7] MACEK, Karel. *Kovové materiály*. V Praze: Nakladatelství ČVUT, 2006. ISBN 80-010-3513-1.
- [8] JANOVEC, Jiří, Petr ZUNA a Karel MACEK. *Fyzikální metalurgie*. Praha: Vydavatelství ČVUT, 2004. ISBN 80-010-2935-2.
- [9] SEDLÁČEK, Vladimír. *Neželezné kovy a slitiny*. Řada hutnické literatury. Praha: Nakladatelství technické literatury, 1979.
- [10] SMALLMAN, R. a R. BISHOP. *Modern physical metallurgy and materials engineering: science, process, applications*. 6th ed. Boston: Butterworth Heinemann, 1999. ISBN 07-506-4564-4.
- [11] HUMPHREYS, F. a M. HATHERLY. *Recrystallization and related annealing phenomena*. 2nd ed. Boston: Elsevier, 2004. ISBN 00-804-4164-5.
- [12] VOJTĚCH, Dalibor. *Kovové materiály*. Praha: Vydavatelství VŠCHT, 2006. ISBN 80-708-0600-1.
- [13] PTÁČEK, Luděk. *Nauka o materiálu I. 2.*, opr. a rozš. vyd. Brno: Akademické nakladatelství CERM, 2003. ISBN 80-720-4283-1.
- [14] ČSN 42 0056: *Tepelné zpracování neželezných kovů a jejich slitin. Rozdělení, názvosloví a definice*. Český normalizační institut, 1993.
- [15] *Metals handbook*. 9th ed. Metals Park, Ohio: American Society for Metals, 1989. ISBN 08-717-0007-7.
- [16] PEREIRA, A.M., J.M. FERREIRA, F.V. ANTUNES a P.J. BÁRTOLO. Analysis of manufacturing parameters on the shear strength of aluminium adhesive single-lap joints. *Journal of Materials Processing Technology*. vol. 210. 2010, **210**(4), 610-617. DOI: 10.1016/j.jmatprotec.2009.11.006. ISSN 09240136. Dostupné z: <https://linkinghub.elsevier.com/retrieve/pii/S0924013609004051>

- [17] ČSN EN ISO 6892-1: *Kovové materiály - Zkoušení tahem - Část 1: Zkušební metoda za pokojové teploty*. Praha: Úřad pro technickou normalizaci, metrologii a státní zkušebnictví, 2017.
- [18] GOLDSTEIN, Joseph. *Scanning electron microscopy and X-ray microanalysis: a text for biologists, materials scientists, and geologists*. New York: Plenum Press, 1981. ISBN 03-064-0768-X.
- [19] ČSN EN ISO 6507-1: *Kovové materiály - Zkouška tvrdosti podle Vickerse - Část 1: Zkušební metoda*. Praha: Úřad pro technickou normalizaci, metrologii a státní zkušebnictví, 2018.

LIST OF FIGURES

Figure 1 – Divide of aluminum alloys [3]	12
Figure 2 - Dependence of yield strength on the grain size of aluminum and copper [9]	20
Figure 3 - Influence of element content on the increase of aluminum strength [9]	20
Figure 4 - Stress for the passage of the dislocation through the particle depending on the particle diameter [8]	21
Figure 5 - Friedel mechanism [7]	22
Figure 6 - Orowan mechanism [7]	23
Figure 7 - Change of selected mechanical properties depending on temperature [12]	25
Figure 8 - Schematic representation of polygonization a) deformed stage, b) recovered substructure [8] ...	27
Figure 9 - Scheme of deformation-induced deflection of the original grain boundary [8]	29
Figure 10 - Theoretical curves of recrystallization kinetics [8]	31
Figure 11 - Progression of recrystallization start t_R and start of precipitation t_P for alloy with concentration c_0 [9]	32
Figure 12 - Slip deformation on the left, twin deformation on the right [8]	35
Figure 13 - Representation of deformation structure formation [13]	37
Figure 14 – The annealing process [1]	39
Figure 15 – EXT sample is shown on the left, HCM sample is shown on the right	46
Figure 16 - Stress–strain curve for the 6082-T6 aluminium alloy [15]	50
Figure 17 - Place of sampling for the tensile test	51
Figure 18 - Values of yield and ultimate strength for samples without heat treatment	52
Figure 19 - Values of yield and ultimate strength for samples with heat treatment	52
Figure 20 - Values of ductility and area restriction for all the samples	53
Figure 21 - Scheme of sample preparation procedure	47
Figure 22 - Area A indicates a transection, Area B indicates a cross section	47
Figure 23 - Example of the sample naming	48
Figure 24 – Surface of the sample 12X_200x	55
Figure 25 - Surface of the sample 22X_200x	55
Figure 26 - Surface of the sample 14X_100x	56
Figure 27 - Surface of the sample 24X_200x	56
Figure 28 - Surface of the sample 17X_50x	57
Figure 29 - Surface of the sample 27X_200x	57
Figure 30 - Core of the sample 12X_200x	58
Figure 31 - Core of the sample 22X_200x	58
Figure 32 - Core of the sample 14X_200x	59
Figure 33 - Core of the sample 24X_200x	59
Figure 34 - Core of the sample 17X_500x	60
Figure 35 - Core of the sample 27X_500x	60
Figure 36 – HAGB and LAGB in the sample 12X_200x	63
Figure 37 - HAGB and LAGB in the sample 22X_200x	63
Figure 38 - HAGB and LAGB in the sample 14X_200x	64
Figure 39 - HAGB and LAGB in the sample 24X_200x	64
Figure 40 - The orientation of the grains in the sample 12X_200x	65
Figure 41 - The orientation of the grains in the sample 22X_200x	65
Figure 42 – The orientation of the grains in the sample 14X_200x	66
Figure 43 - The orientation of the grains in the sample 24X_200x	66
Figure 44 - The hardness values for extruded samples in transection	70
Figure 45 - The hardness values for extruded samples in cross section	71
Figure 46 - The hardness values for HCM samples in transection	73
Figure 47 - The hardness values for HCM samples in cross section	74
Figure 48- The hardness values for all the samples without a heat treatment	75
Figure 49 - The hardness values for all the samples with a heat treatment	75
Figure 50 - Progression of hardness values depending on load for sample 12PRX	76

LIST OF TABLES

Table 1 - Selected physical properties of aluminum [1]	11
Table 2 – The thermal expansion values at different temperature intervals [1]	12
Table 3 - Maximum content of alloying elements [1]	13
Table 4 – Solid phases in the Al-Mg-Si system [1]	14
Table 5 - Alloying intervals for wrought alloys 6000 series [1]	15
Table 6 - Chemical composition of EN AW 6082 alloy in weight % [6]	16
Table 7 - Mechanical properties of alloy EN AW 6082 depending on the heat treatment [6]	17
Table 8 - Influence of alloying elements on substitutional reinforcement of aluminum [1]	21
Table 9 – Input parameters of the semi-finished products	43
Table 10 – Parameters of deformation	44
Table 11 – Results of the tensile test	51
Table 12 - The hardness of the extruded samples in transection	69
Table 13 - The hardness of the extruded samples in cross section	70
Table 14 – Increase of hardness in extruded samples	71
Table 15 - The hardness of the HCM semi-finished products in transection	72
Table 16 - The hardness of the HCM semi-finished products in cross section	73
Table 17 - Increase of hardness in HCM samples	74
Table 18 - Increase of hardness in both semi-finished products	76